São Paulo J. Math. Sci. (2015) 9:1–36
DOI 10.1007/s40863-015-0001-9

Symmetry methods in mathematical biology

Martin Golubitsky[1] · **Ian Stewart**[2]

Published online: 19 May 2015

Abstract Many biological systems have aspects of symmetry. Symmetry is formalized using group theory. This theory applies not just to the geometry of symmetric systems, but to their dynamics. The basic ideas of symmetric dynamics and bifurcation theory are applied to speciation, animal locomotion, the visual cortex, pattern formation in animal markings and geographical location, and the geometry of virus protein coats.

Keywords Symmetry · Biology · Network · Bifurcation · Speciation · Locomotion · Hallucination · Neuroscience · Virus

1 Introduction

The formal mathematical theory of symmetry has many uses in the construction and analysis of models of biological forms and processes. We begin with some simple models of population dynamics including territorial effects. We then describe applications to speciation, animal locomotion, the visual cortex, pattern formation in animal markings, geographical location, and virus structure.

The mathematical setting for symmetry is group theory. A group is a collection of transformations that preserve specified forms or structures. In this setting, an object or system does not just possess symmetry: it may possess several different symmetries. Group theory characterizes the interplay between these. The symmetries of an object

✉ Ian Stewart
i.n.stewart@warwick.ac.uk

[1] Mathematical Biosciences Institute, Ohio State University, 364 Jennings Hall, Columbus, OH 43210, USA

[2] Mathematics Institute, University of Warwick, Coventry CV4 7AL, UK

or system have profound effects on its form, function, and behavior. Merely knowing that the atomic structure of a crystal is a lattice implies that the crystal's rotational symmetries can be of order 2, 3, 4, or 6, but not 5 or any number greater than 6. This "crystallographic restriction" is a group-theoretic consequence of lattice geometry in two and three dimensions.

In the physical sciences, symmetries are often exact, or so close to exact that it is standard to model them that way. In the life sciences, exact symmetry is rare. The capsids of icosahedral viruses are symmetric with a high degree of precision, because their form is determined by molecular forces, but even there the interior of the virus lacks the symmetry of its protein coat. In most biological systems, symmetries are at best approximate, so their use in models is an idealization. In mathematical models of a network of neurons, for example, it is common to treat neurons of the same general kind as identical, so that the parameters in the corresponding equations are the same. When modeling speciation, the actual close resemblance between creatures of the same species is idealized to "identical". Idealizations of this kind are useful because they simplify the mathematical analysis, and because systems with approximate symmetries usually resemble idealized symmetric models more closely than they resemble typical asymmetric models.

Symmetry methods, making explicit use of group theory, can be viewed as a toolkit of systematic techniques for analyzing pattern formation. In biological settings they are most appropriate in contexts where more or less regular patterns are observed. Those patterns may be visual, for example animal markings; they may be dynamic, as in animal locomotion; or they may be on a more abstract structural level, as in speciation. We consider only regular patterns and dynamics, specifically, steady states and spatially or temporally periodic structures. Symmetry can also force the occurrence of heteroclinic cycles [47], which are equilibria of saddlepoint type joined by their separatrices. When such cycles are present, the system will appear to be in equilibrium for a time, but then move relatively quickly to another apparent equilibrium. Such dynamics can be highly complex, even when the system is not chaotic [28]. Heteroclinic cycles can occur in particular in population models [49,94]. There is also a well-developed theory of symmetric chaos, which leads to less regular patterns with their own hidden symmetries [29,30,39].

2 Motivating examples in population dynamics

We begin with a simple warm-up problem, which introduces some basic features of symmetric dynamics. More realistic models with the same symmetries would exhibit similar phenomena.

Example 2.1 A species of birds occupies two neighboring islands, of similar sizes and with similar habitats. The two bird populations at time t are proportional to $P + x(t)$, $P + y(t)$, where P is a fixed reference population chosen so that $P + x(t) \geq 0$ and $P + y(t) \geq 0$ for all relevant t. The constant of proportionality is not specified here. Birds reproduce on each island and migrate between them. A simple model of the populations, with nonlinear population growth and linear migration, is:

Table 1 Equilibria and their stabilities for Eq. (1)

x	y	Eigenvalues of J	Stability
0	0	7, 3	Unstable
$\sqrt{7}$	$\sqrt{7}$	$-14, -18$	Stable
$-\sqrt{7}$	$-\sqrt{7}$	$-14, -18$	Stable
$\sqrt{3}$	$-\sqrt{3}$	$-2, -6$	Stable
$-\sqrt{3}$	$\sqrt{3}$	$-2, -6$	Stable
1	-2	$(-5+\sqrt{97})/2, (-5-\sqrt{97})/2$	Unstable
-1	2	$(-5+\sqrt{97})/2, (-5-\sqrt{97})/2$	Unstable
2	-1	$(-5+\sqrt{97})/2, (-5-\sqrt{97})/2$	Unstable
-2	1	$(-5+\sqrt{97})/2, (-5-\sqrt{97})/2$	Unstable

$$\begin{aligned} x'(t) &= kx(t) - x(t)^3 + a(y(t) - x(t)) \\ y'(t) &= ky(t) - y(t)^3 + a(x(t) - y(t)) \end{aligned} \tag{1}$$

Here k is the growth rate when the population is small, the terms $-x(t)^3, -y(t)^3$ are nonlinear density-dependent terms that limit the population size, and a is the migration rate.

To keep the calculations simple, let the parameters be $k = 7, a = 2$. At an equilibrium, $x(t)$ and $y(t)$ are independent of t, and we denote their constant values by x and y. The population equilibria are the solutions of $kx - x^3 + a(y - x) = 0 = ky - y^3 + a(x - y)$. Table 1 shows these, together with their stabilities, determined by the eigenvalues of the Jacobian matrix

$$J = \begin{pmatrix} k - a - 3x^2 & a \\ a & k - a - 3y^2 \end{pmatrix} \tag{2}$$

An equilibrium is stable if the eigenvalues of J at the equilibrium have negative real parts [56, II.7]. Since $(-5 + \sqrt{97})/2 > 0$, the final four equilibria are unstable.

These results exemplify three typical phenomena in symmetric systems of ODEs:

Multiplicity Nonlinear differential equations often have multiple equilibria. Bézout's Theorem [32] states that, subject to technical hypotheses, a system of two independent polynomial equations of degrees m and n in two variables has at most mn solutions. Table 1 lists 9 equilibria in total; by Bézout's Theorem, this is the maximum number possible with two cubic equations.

Symmetrically related states Multiplicity interacts with symmetry: equilibria occur in sets, each having the same eigenvalues of J, Table 1. These sets are related by symmetries. The equations are preserved by four changes of coordinates:

$$(x, y) \mapsto (x, y) \quad (x, y) \mapsto (y, x) \quad (x, y) \mapsto (-x, -y) \quad (x, y) \mapsto (-y, -x) \tag{3}$$

The image of any solution under any of these transformations is also a solution, and Jacobians at symmetrically related equilibria have the same eigenvalues because they are similar, or conjugate, as matrices.

Spontaneous symmetry-breaking Solutions need not have the same symmetries as the equations. An equilibrium with all four symmetries must be of the form $(0, 0)$, which is valid only for the first solution in Table 1. The remaining equilibria are of three kinds: (x, x) where $x \neq 0$, $(x, -x)$ where $x \neq 0$, and (x, y) where $y \neq \pm x$. The first type has symmetry $(x, y) \mapsto (y, x)$. The second type has symmetry $(x, y) \mapsto (-y, -x)$. The third type has only the trivial symmetry.

This phenomenon—solutions with less symmetry than the equations—is called *spontaneous symmetry-breaking* [101]. "Spontaneous" indicates that the symmetry of the equations is not changed, only that of solutions. The unqualified term "symmetry-breaking" is also used to refer to small asymmetric perturbations of the equations. Spontaneous symmetry-breaking is a common phenomenon in symmetric dynamics, and one of the main sources of pattern formation. It can also occur for periodic and chaotic states. We discuss the periodic case in Sect. 3.

Example 2.2 The symmetry $(x, y) \mapsto (y, x)$ is a consequence of our assumption that conditions on the two islands are identical, and that the rate of migration between them is the same in both directions. With more than two identical islands, similar symmetries arise. In contrast, the symmetry $(x, y) \mapsto (-x, -y)$ is artificial, created by the cubic nonlinearity in the model of isolated population growth. To remove this symmetry we introduce a small quadratic term. The model for three islands then takes the form:

$$\begin{aligned} x'(t) &= kx(t) - x(t)^2/8 - x(t)^3 + a(y(t) + z(t) - 2x(t)) \\ y'(t) &= ky(t) - y(t)^2/8 - y(t)^3 + a(x(t) + z(t) - 2y(t)) \\ z'(t) &= kz(t) - z(t)^2/8 - z(t)^3 + a(x(t) + y(t) - 2z(t)) \end{aligned} \tag{4}$$

The analogous table, computed numerically for parameter values $k = 10, a = 1$, is Table 2.

Equation (4) is symmetric under all permutations of x, y, z. There are six such permutations, forming the symmetric group $\mathbb{S}_3$. There are 27 real equilibria, the maximum multiplicity permitted by Bézout's Theorem. Small asymmetric perturbations also have 27 real equilibria. The 27 equilibria divide into ten symmetry classes. In the first three of these, the equilibria are fully symmetric, of the form (x, x, x). In the next six, the equilibria are of the form (x, y, y), (y, x, y) and (y, y, x), so each equilibrium is invariant under a transposition, (23), (13) and (12), respectively. In the final class, all three variables are distinct, and each equilibrium has trivial symmetry.

It would be easy to assume that because all three islands provide the same habitat, and the same species of birds inhabits each, the populations should be identical on each island. Some equilibria are of this form. However, the model has stable equilibria that are *not* of this form: an example of spontaneous symmetry-breaking. This phenomenon is common in symmetric systems of equations. What makes it possible is the presence of nonlinear terms. A symmetric linear system of ODEs $x'(t) = Ax(t)$ has a unique

Table 2 Equilibria and their stabilities for Eq. (4)

x	y	z	Eigenvalues of J	Stability
0	0	0	10, 7, 7	Unstable
3.10	3.10	3.10	−22.61, −22.61, −19.61	Stable
−3.23	−3.23	−3.23	−23.40, −23.40, −20.40	Stable
2.26	−2.93	−2.93	−18.04, −16.29, −7.71	Stable
−2.93	2.26	−2.93	−18.04, −16.29, −7.71	Stable
−2.93	−2.93	2.26	−18.04, −16.29, −7.71	Stable
−2.46	2.79	2.79	−17.01, −15.35, −9.16	Stable
2.79	−2.46	2.79	−17.01, −15.35, −9.16	Stable
2.79	2.79	−2.46	−17.01, −15.35, −9.16	Stable
−0.77	2.89	2.89	−18.84, −16.92, 6.49	Unstable
2.89	−0.77	2.89	−18.84, −16.92, 6.49	Unstable
2.89	2.89	−0.77	−18.84, −16.92, 6.49	Unstable
−2.85	0.32	0.32	−15.76, 8.69, 6.61	Unstable
0.32	−2.85	0.32	−15.76, 8.69, 6.61	Unstable
0.32	0.32	−2.85	−15.76, 8.69, 6.61	Unstable
2.73	−0.30	−0.30	−15.07, 8.88, 6.80	Unstable
−0.30	2.73	−0.30	−15.07, 8.88, 6.80	Unstable
−0.30	−0.30	2.73	−15.07, 8.88, 6.80	Unstable
0.84	−3.02	−3.02	−19.54, −17.63, 5.76	Unstable
−3.02	0.84	−3.02	−19.54, −17.63, 5.76	Unstable
−3.02	−3.02	0.84	−19.54, −17.63, 5.76	Unstable
2.57	0.02	−2.72	−14.12, −11.99, 8.09	Unstable
2.57	−2.72	0.02	−14.12, −11.99, 8.09	Unstable
0.02	2.57	−2.72	−14.12, −11.99, 8.09	Unstable
0.02	−2.72	2.57	−14.12, −11.99, 8.09	Unstable
−2.72	2.57	0.02	−14.12, −11.99, 8.09	Unstable
−2.72	0.02	2.57	−14.12, −11.99, 8.09	Unstable

equilibrium provided the matrix of coefficients A is non-singular. So uniqueness of the equilibrium is "generic" or "typical", in the sense that any system with non-unique equilibria can be changed to one with unique equilibria by making an arbitrarily small perturbation of the terms appearing in the equation, that is, of the matrix A. Uniqueness forces that equilibrium to be fully symmetric. However, equilibria of symmetric PDEs need not be fully symmetric, even in the linear case.

Traces of the symmetry of the equations remain, however, even when symmetry is broken. In place of a single fully symmetric solution, there is a *set* of symmetrically related solutions. In Example 2.2, the symmetry group of the equations is large enough for some solutions to have nontrivial symmetry, forming a proper subgroup of the symmetry group of the equations. We explain why this happens in Sect. 3, which describes some basic properties of symmetric equations.

3 Symmetries and group theory

Solutions of systems of ODEs can behave in many different ways. The most basic classification includes five types: equilibrium, periodic, heteroclinic, quasiperiodic, and chaotic [47]. At an equilibrium the solution remains constant for all time. For a periodic state it repeats the same behavior indefinitely at regularly spaced intervals of time (the period).

A basic question is: *given the symmetries of the equation, what are the possible symmetries of solutions?* We answer this question for equilibria and periodic states. In the periodic case, there is an extra source of symmetry: phase shifts (time translations) on solutions. Any autonomous ODE has time-translation symmetry: if $v(t)$ is a solution, so is $v(t+\theta)$, for any constant θ. Equilibria are the states that do not break this time-translation symmetry; periodic solutions break it, but not completely. Time-reversal symmetry, in which t becomes $-t$, usually accompanied by a spatial symmetry, may also occur [7,69].

In order to answer the basic question above, we first recall some standard ideas concerning groups, equivariant maps (which define symmetric ODEs) and related topics [39,42].

3.1 Groups

The formal setting for the analysis of symmetric ODEs employs the notion of a group. The usual definition specifies a short list of axioms [72]. Here we take a more concrete view and define a *group* to be a set Γ of invertible transformations of some set V such that, if f, g are in the set then so is their *composition* fg, defined by

$$fg(v) = f(g(v)) \quad v \in V \tag{5}$$

For most of the groups we discuss, V is a finite-dimensional real vector space and the transformations are linear. Technically, distinct elements of Γ may correspond to the same linear transformation. This occurs in a few examples below.

We introduce some standard groups.

The *cyclic group* $\mathbb{Z}_n$ consists of all rotations of the plane about the origin through angles $\frac{2k\pi}{n}$, where $0 \le k < n$ is an integer. It is the group of all rotational symmetries of a regular n-sided polygon.

The *dihedral group* $\mathbb{D}_n$ also acts on the plane. It consists of $\mathbb{Z}_n$, together with reflections in lines through the origin at angles $\frac{k\pi}{n}$, where $0 \le k < n$ is an integer. It is the group of all symmetries of a regular n-sided polygon.

The *special orthogonal group* $\mathbb{SO}(2)$ in the plane consists of all rotations about the origin. It is the group of rotational symmetries of the unit circle.

The *orthogonal group* $\mathbb{O}(2)$ in the plane consists of all rotations about the origin and all reflections in lines through the origin. It is the group of all symmetries of the unit circle.

The *Euclidean group* $\mathbb{E}(2)$ consists of all rigid motions of the plane: combinations of translations, rotations, and reflections. This is not a group of linear transforma-

tions, because rigid motions do not in general fix the origin. It consists of affine transformations.

The *special orthogonal group* $\mathbb{SO}(3)$ in $\mathbb{R}^3$ consists of all rotations about the origin. It is the group of all rotational symmetries of the unit sphere.

The *orthogonal group* $\mathbb{O}(3)$ in $\mathbb{R}^3$ consists of all rotations about the origin, all reflections in planes through the origin, and combinations of these transformations such as minus the identity: $(x, y, z) \mapsto (-x, -y, -z)$. It is the group of all symmetries of the unit sphere.

The *symmetric group* $\mathbb{S}_n$ consists of all permutation matrices in $\mathbb{R}^n$, that is, all linear transformations

$$\sigma(v_1, \ldots, v_n) = (v_{\sigma^{-1}(1)}, \ldots, v_{\sigma^{-1}(n)}) \tag{6}$$

We use σ^{-1} so that $\sigma\tau(v) = \sigma(\tau(v))$.

The *order* of a finite group is the number of elements that it contains. Here $\mathbb{Z}_n$ has order n; $\mathbb{D}_n$ has order $2n$; $\mathbb{S}_n$ has order $n!$ The other groups are infinite. The groups $\mathbb{SO}(2)$, $\mathbb{O}(2)$, $\mathbb{SO}(3)$, $\mathbb{O}(3)$ are compact Lie groups [85]; informally, the entries in the matrices are uniformly bounded. The Euclidean group $\mathbb{E}(2)$ is not compact because it contains translations through arbitrarily large distances.

3.2 Equivariant maps

We formalize the concept of a symmetric system of equations.

Let Γ be a group of linear transformations acting on a vector space $V = \mathbb{R}^n$. A smooth map $f : V \to V$ is Γ-*equivariant* if

$$f(\gamma v) = \gamma f(v) \tag{7}$$

for all $\gamma \in \Gamma$, $v \in V$. The map f determines a Γ-*equivariant ODE*:

$$v'(t) = f(v(t)) \tag{8}$$

For example, the system in Eq. (4) is $\mathbb{S}_3$-equivariant, where the group $\mathbb{S}_3$ acts on $\mathbb{R}^3$ by permutations of the variables as above. Throughout the paper we often consider a system of ODEs to be a single vector ODE, so "ODE" may refer to a system.

The equivariance condition Eq. (7) guarantees that γ maps solutions to solutions. This condition is required here, rather than group invariance $f(\gamma v) = f(v)$, because the equations are not preserved by invariant maps. For example, the transposition (12) that swaps x and y transforms Eq. (4) so that

$$f(\gamma v) = \begin{pmatrix} ky - y^2/8 - y^3 + a(x + z - 2y) \\ kx - x^2/8 - x^3 + a(y + z - 2x) \\ kz - z^2/8 - z^3 + a(x + y - 2z) \end{pmatrix} \tag{9}$$

where $v = (x, y, z)$. This leads to the equation

$$x'(t) = ky(t) - y(t)^2/8 - y(t)^3 + a(x(t) + z(t) - 2y(t)) \tag{10}$$

for $x(t)$, instead of preserving the first equation in (4). To restore the original system of equations we must also permute the components of f according to the same transposition (12). The same holds for the other permutations in $\mathbb{S}_3$. Requiring the permutation to act on the components of Eq. (4), as well as the variables, preserves the system of ODEs. This leads to a key feature of equivariant ODEs:

Proposition 3.1 *If $v(t)$ is a solution of Eq. (7) then so is $\gamma v(t)$ for all $\gamma \in \Gamma$.*

Proof

$$(\gamma v(t))' = \gamma v(t)' = \gamma f(v(t)) = f(\gamma v(t)) \tag{11}$$

Equivariance is necessary for this property to hold, as well as sufficient [39]. Proposition 3.1 explains why the solutions in Tables 1 and 2 occur in symmetrically related classes. □

3.3 Isotropy subgroups and fixed-point subspaces

We explain why some of these classes contain more solutions than others. It turns out that the more symmetry any given solution has, the smaller the corresponding symmetry class is. To formalize this statement, we first introduce some terminology.

Definition 3.2 If $v \in V$ then the *isotropy subgroup* of v is

$$\Sigma_v = \{\sigma \in \Gamma : \sigma v = v\} \tag{12}$$

If $v(t)$ is a solution of (8) then the *isotropy subgroup* of $v(t)$ is

$$\Sigma_{v(t)} = \{\sigma \in \Gamma : \sigma v(t) = v(t) \quad \forall t \in \mathbb{R}\} \tag{13}$$

If $\Sigma \subseteq \Gamma$ is a subgroup of Γ, then its *fixed-point subspace* is

$$\mathrm{Fix}(\Sigma) = \{v \in V : \sigma v = v \quad \forall \sigma \in \Sigma\} \tag{14}$$

Example 3.3 Suppose that Γ is the symmetry group of Eq. (1), consisting of the transformations

$$I(x, y) = (x, y) \tag{15}$$
$$\sigma(x, y) = (y, x) \tag{16}$$
$$-I(x, y) = (-x, -y) \tag{17}$$
$$-\sigma(x, y) = (-y, -x) \tag{18}$$

The subgroups of Γ and their fixed-point spaces are shown in Table 3.

In this example, every subgroup is an isotropy subgroup, with the exception of $\{I, -I\}$. This is excluded because the only point it fixes is the origin, but the subgroup that fixes the origin is the whole of Γ. It is common for some subgroups not to be isotropy subgroups, depending on the group concerned.

Table 3 Subgroups of the symmetry group and their fixed-point spaces for Eq. (1)

Subgroup	Fixed-point space
$\{I\}$	$\mathbb{R}^2$
$\{I, \sigma\}$	$\{(x, x)\}$
$\{I, -I\}$	$\{(0, 0)\}$
$\{I, -\sigma\}$	$\{(x, -x)\}$
Γ	$\{(0, 0)\}$

3.4 Symmetries of equilibria

We answer the basic question of symmetry-breaking for equilibria: given the symmetry group Γ of the ODE, what are the possible symmetries of equilibria? The answer is: the isotropy subgroups of Γ. This characterizes the subgroups in a computable manner, and it makes the point that some subgroups may not occur in this context. In Example 3.3, the subgroup $\{I, -I\}$ is not an isotropy subgroup. Later examples illustrate how this simple observation can lead to systematic classifications of patterns.

The isotropy subgroup of a point v or trajectory $v(t)$ determines the symmetries of that point or trajectory. The fixed-point space of a subgroup Σ contains all solutions with symmetry Σ, and can be used to find such solutions because fixed-point spaces are invariant under the dynamics. The proof is a one-line calculation, which shows that for any Γ-equivariant f and any subgroup $\Sigma \subseteq \Gamma$,

$$f(\mathrm{Fix}(\Sigma)) \subseteq \mathrm{Fix}(\Sigma) \tag{19}$$

This implies that we can find all solutions of Eq. (8) that have symmetry (at least) Σ by restricting f to $\mathrm{Fix}(\Sigma)$ and considering the ODE on $\mathrm{Fix}(\Sigma)$ with vector field $f|_{\mathrm{Fix}(\Sigma)}$.

Example 3.4 Consider the 3-island model in Eq. (4). The isotropy subgroups include the subgroup Σ generated by the transposition (12), with fixed-point subspace $\{(x, x, z)\}$. The three equations, restricted to this subspace, take the form

$$\begin{aligned} x'(t) &= kx(t) - x(t)^2/8 - x(t)^3 + a(x(t) + z(t) - 2x(t)) \\ y'(t) &= kx(t) - x(t)^2/8 - x(t)^3 + a(x(t) + z(t) - 2x(t)) \\ z'(t) &= kz(t) - z(t)^2/8 - z(t)^3 + a(x(t) + x(t) - 2z(t)) \end{aligned} \tag{20}$$

The first two equations are identical, consistent with the invariance of $\mathrm{Fix}(\Sigma)$. We can ignore the second equation and compute the eigenvalues of the Jacobian of the *reduced ODE* given by the first and third equations, which is

$$\hat{J} = \begin{pmatrix} k - \frac{x}{4} - 3x^2 - a & a \\ 2a & k - \frac{z}{4} - 3z^2 - 2a \end{pmatrix} \tag{21}$$

The result is Table 4. Comparing with Table 2, we see that the method locates all equilibria of Eq. (4) of the form $\{(x, x, z)\}$. Moreover, the eigenvalues of $\hat{J}$ are two

Table 4 Equilibria and their stabilities for Eq. (20)

x	z	Eigenvalues of J	Stability
0	0	10, 7	Unstable
3.10	3.10	−22.61, −19.61	Stable
−3.23	−3.23	−23.40, −20.40	Stable
−2.93	2.26	−16.29, −7.71	Stable
2.79	−2.46	−15.35, −9.16	Stable
2.89	−0.77	−16.92, 6.49	Unstable
0.32	−2.85	−15.76, 8.69	Unstable
−0.30	2.73	−15.07, 8.88	Unstable
−3.02	0.84	−17.63, 5.76	Unstable

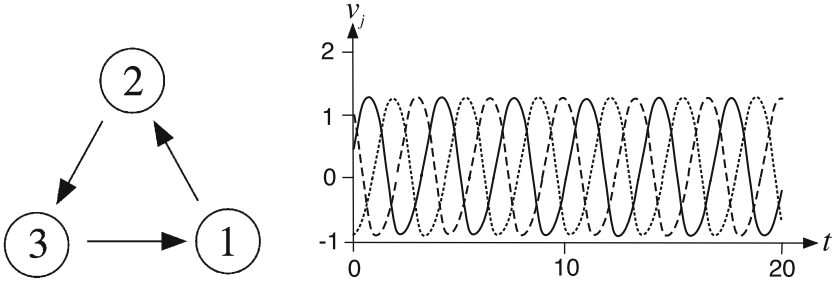

Fig. 1 *Left* Ring of Fitzhugh–Nagumo neurons with unidirectional coupling. *Right* Periodic oscillations of the 3-cell ring exhibiting a $\frac{1}{3}$ period out of phase periodic solution. Time series of v_1 (*thick solid*), v_2 (*dotted*), v_3 (*dashed*)

of the eigenvalues of J. This happens because $\mathrm{Fix}(\Sigma)$ is invariant under J, a general result that follows from (19) because J is Γ-equivariant.

In general, unstable equilibria of a restricted system are also unstable for the full system, but the converse need not be true since stability in the full space depends on the "transverse" eigenvalues of J: those that do not correspond to eigenvalues of $\hat{J}$. In the example of Eq. (20) the transverse eigenvalues do not change the stabilities.

3.5 Symmetries of Periodic States

We discuss analogous ideas for periodic solutions, beginning with a simple example. Periodic states are particularly common in neuroscience, so we will use a model of three Fitzhugh–Nagumo equations [31,81] coupled unidirectionally in a ring, as in Fig. 1, left. For a single neuron, the model involves a membrane potential v and a surrogate w for an ionic current. The dynamic of a single neuron is determined by the ODE

$$\begin{aligned} v'(t) &= v(t)(a - v(t))(v(t) - 1) - w(t) \\ w'(t) &= bv(t) - \gamma w(t) \end{aligned} \tag{22}$$

where a, b, γ are parameters and $0 < a < 1, b > 0, \gamma > 0$.

Example 3.5 In the ring, cells are coupled unidirectionally, and each receives an input from one neighboring cell. We model each cell using a copy of Eq. (22) and incorporate the coupling by adding a voltage term to each equation:

$$\begin{aligned} v_1'(t) &= v_1(t)(a - v_1(t))(v_1(t) - 1) - w_1(t) - cv_2(t) \\ w_1'(t) &= bv_1(t) - \gamma w_1(t) \\ v_2'(t) &= v_2(t)(a - v_2(t))(v_2(t) - 1) - w_2(t) - cv_3(t) \\ w_2'(t) &= bv_2(t) - \gamma w_2(t) \\ v_3'(t) &= v_3(t)(a - v_3(t))(v_3(t) - 1) - w_3(t) - cv_1(t) \\ w_3'(t) &= bv_3(t) - \gamma w_3(t) \end{aligned} \tag{23}$$

The symmetry group is $\mathbb{Z}_3$ generated by the 3-cycle (123) acting on pairs (v_j, w_j).

The origin is a stable equilibrium for the full six-dimensional system when, for example, $a = b = \gamma = 0.5$ and $c = 0.8$. Hence the cells are trivially synchronous. When, for example, $a = b = \gamma = 0.5$ and $c = 2$, the three-cell system has a stable periodic solution with successive cells one third of the period out of phase. Figure 1, right shows the pattern for the v_j; the same pattern occurs for the w_j. This is an instance of what Hoppensteadt [51] calls "rosette phase locking". Another term is *discrete rotating wave*.

This phenomenon is a group-theoretic consequence of the symmetry of the three-cell network. The specific choice of model realizes a pattern typical of many $\mathbb{Z}_3$-symmetric systems. The new feature, compared to equilibria, is that the periodic state has *spatio-temporal* symmetry. If the period is T, the solution satisfies the phase relationships

$$v_2(t) = v_1\left(t - \frac{T}{3}\right) \quad v_3(t) = v_1\left(t - \frac{2T}{3}\right) \tag{24}$$

for all t. The solution is invariant if we permute the labels using the 3-cycle $\rho = (123)$ acting as in Eq. (6) and shift phase by $\frac{T}{3}$. It satisfies

$$\rho v\left(t + \frac{T}{3}\right) = v(t) \tag{25}$$

and in group-theoretic terms it is fixed by the element $(\rho, \frac{T}{3}) \in \Gamma \times \mathbb{S}^1$, where $\mathbb{S}^1$ is the circle group of phase shifts; that is, time translations modulo T.

In the case of synchrony, the diagonal

$$\Delta = \{(v_1, w_1, v_2, w_2, v_3, w_3) : v_1 = v_2 = v_3, w_1 = w_2 = w_3\} \tag{26}$$

is a flow-invariant subspace. This also follows from Eq. (19) because $\Delta = \mathrm{Fix}(\mathbb{S}_3)$. Two cells are *synchronous* if their time series are identical, so the invariance of Δ implies that synchrony should be expected in $\mathbb{Z}_3$-symmetric three-cell systems.

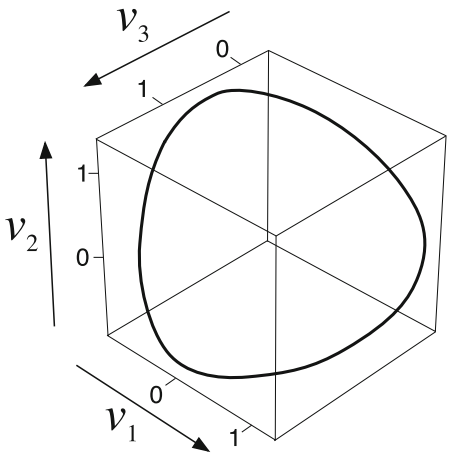

Fig. 2 Setwise $\mathbb{Z}_3$ symmetry of periodic trajectory of three coupled Fitzhugh–Nagumo neurons

Phase-locking is also a natural consequence of symmetry, though it has a subtler cause, not directly related to a fixed-point space. To see how a phase-locked state can arise from symmetry, suppose that $v(t)$ is a T-periodic solution to (8) and that γ is a symmetry. Then either $\gamma v(t)$ is a different periodic trajectory from $v(t)$, or it is the same trajectory. In the latter case, the only difference is a time-translation. That is, $\gamma v(0) = v(\theta)$ for some θ, and uniqueness of solutions of ODEs implies that $\gamma v(t) = v(t+\theta)$ for all t. In the three-cell system where $v = (x_1, x_2, x_3)$, applying ρ three times implies that $3\theta \equiv 0 \pmod{T}$. Hence $\theta = 0$, $\frac{T}{3}$, or $\frac{2T}{3}$. Since ρ is the permutation (123) it follows that $x_2(t) = x_1(t)$ when $\theta = 0$ (synchrony) and $x_2(t) = x_1(t+\frac{T}{3})$ when $\theta = \frac{T}{3}$ and $x_2(t) = x_1(t+\frac{2T}{3})$ when $\theta = \frac{2T}{3}$ (phase-locking).

Figure 2 shows the trajectory $(v_1(t), v_2(t), v_3(t))$ in $\mathbb{R}^3$, viewed from a point very close to the main diagonal (to avoid confusing the perspective). The periodic cycle is shaped like a curved equilateral triangle, corresponding to the setwise $\mathbb{Z}_3$ symmetry.

Discrete rotating waves can occur in rings of other sizes, provided the cells are identical and coupled in a symmetric fashion. For rings with n cells, the phase shifts are integer multiples of $\frac{2\pi}{n}$. For example the nephron model of Mosekilde et al. [77] is $\mathbb{Z}_2$-symmetric and can have periodic states that are a half-period out of phase.

A periodic trajectory has *two* symmetry groups: the group H of transformations that fix the periodic orbit but change its time-parametrization, and the group K of transformations that fix each point in the periodic orbit, and thus leave its time-parametrization unchanged. The pairs of subgroups (H, K) of Γ that can arise as setwise and pointwise symmetries of a periodic state of a Γ-equivariant ODE are characterized by the H/K Theorem of Buono and Golubitsky [6]. This states that for a given finite group Γ there exists a Γ-equivariant ODE with a periodic state determining a pair of subgroups (H, K) if and only if:

(1) H/K is cyclic;
(2) K is an isotropy subgroup of Γ;
(3) $\dim \mathrm{Fix}(K) \geq 2$, and if the dimension equals 2 then either $H = K$ or H is the normalizer of K;
(4) H fixes a connected component of $\mathrm{Fix}(K) \setminus \bigcup_{\gamma \notin K} \mathrm{Fix}(\gamma) \cap \mathrm{Fix}(K)$.

Item (4) is a technical condition on the geometry of the action of Γ. The normalizer of a subgroup H of Γ is the largest subgroup Δ such that H is a normal subgroup of Δ. The main point of the H/K Theorem is that the pairs (H, K) that are associated with a periodic state are constrained in a precise manner and can be classified group-theoretically, for any given Γ.

We call K the group of *spatial symmetries* of the periodic state and H the group of *spatio-temporal symmetries*. The cyclic group H/K acts on the state by phase shifts. If its order is p these are shifts by integer multiples of T/p where T is the period. For example, the discrete rotating wave in Fig. 2, right has $H = \mathbb{Z}_3$, $K = \mathbf{1}$, so trivially $H/K \cong \mathbb{Z}_3$.

3.6 Local bifurcations: steady state

Isotropy subgroups and the H/K Theorem classify the symmetry-breaking equilibria and periodic patterns that *can* arise in equivariant ODEs, but they do not tell us which ones *do* arise for specific equations. They provide a catalogue of possible symmetries; specific systems choose from this catalogue. A useful method for proving that particular choices actually occur is bifurcation theory, which studies how solutions of a parametrized family of ODEs change as the parameter varies. Here we consider only local bifurcations, in which a stable equilibrium loses stability as a single parameter λ varies. In steady state bifurcation, new equilibria arise, and generically these form one or more "branches"—continuous curves in $V \times \mathbb{R} = \{(v, \lambda)\}$. In Hopf bifurcation, we find a branch or branches of periodic states.

Example 3.6 We investigate how the equilibria of Eq. (1) vary with the parameters a, k. Bearing in mind that $a > 0$, we can scale the parameters, variables, and time to set $a = 1$, by defining

$$X = x/\sqrt{a} \quad Y = y/\sqrt{a} \quad T = at \quad K = k/a \tag{27}$$

Then Eq. (1) becomes

$$\begin{aligned} X'(T) &= KX(T) - X(T)^3 + (Y(T) - X(T)) \\ Y'(T) &= KY(T) - Y(T)^3 + (X(T) - Y(T)) \end{aligned} \tag{28}$$

Equilibria (X, Y) are solutions of

$$KX - X^3 + (Y - X) = 0 \quad KY - Y^3 + (X - Y) = 0 \tag{29}$$

We use K as the bifurcation parameter, and rewrite the sum and difference of these equations to yield the equivalent equations

$$(X + Y)(X^2 - XY + Y^2 - K) = 0 \tag{30}$$

$$(X - Y)(X^2 + XY + Y^2 - K + 2) = 0 \tag{31}$$

Therefore the solutions are of four kinds:

$$X = 0 \quad \text{and} \quad Y = 0 \tag{32}$$
$$Y = -X \quad \text{and} \quad X^2 + XY + Y^2 - K + 2 = 0 \tag{33}$$
$$Y = X \quad \text{and} \quad X^2 - XY + Y^2 - K = 0 \tag{34}$$
$$X^2 + XY + Y^2 = K - 2 \quad \text{and} \quad X^2 - XY + Y^2 = K \tag{35}$$

In Eq. (33), $X^2 = K - 2$ so

$$X = \pm\sqrt{K-2} \quad Y = \mp\sqrt{K-2} \tag{36}$$

In Eq. (34), $X^2 = K$ so

$$X = \pm\sqrt{K} \quad Y = \pm\sqrt{K}. \tag{37}$$

Equation (35) is equivalent to $X^2 + Y^2 = K - 1$ and $XY = -1$, the intersection of a circle (when $K > 1$) and a hyperbola. Real solutions exist for $K \geq 3$. They occur as a symmetrically related set of four, except that when $K = 3$ this set reduces to a pair. This set of solutions is bounded away from the origin. The solutions are

$$X = \left(\tfrac{1}{2}(K - 1 + S)\right)^{1/2} \quad Y = -\left(\tfrac{1}{2}(K - 1 - S)\right)^{1/2} \tag{38}$$
$$X = \left(\tfrac{1}{2}(K - 1 - S)\right)^{1/2} \quad Y = -\left(\tfrac{1}{2}(K - 1 + S)\right)^{1/2} \tag{39}$$
$$X = -\left(\tfrac{1}{2}(K - 1 + S)\right)^{1/2} \quad Y = \left(\tfrac{1}{2}(K - 1 - S)\right)^{1/2} \tag{40}$$
$$X = -\left(\tfrac{1}{2}(K - 1 - S)\right)^{1/2} \quad Y = \left(\tfrac{1}{2}(K - 1 + S)\right)^{1/2} \tag{41}$$

where

$$S = \sqrt{(K+1)(K-3)} \tag{42}$$

We plot the equilibria against K in Fig. 3. The branch given by Eq. (35) is a *secondary bifurcation* from the *primary 2 branch* determined by Eq. (33); that is, it arises when the primary branch becomes unstable.

Consider a 1-parameter family of maps $f : \mathbb{R}^n \times \mathbb{R} \to \mathbb{R}^n$ satisfying the equivariance condition

$$f(\gamma x, \lambda) = \gamma f(x, \lambda) \tag{43}$$

for all $x \in \mathbb{R}^n, \lambda \in \mathbb{R}$. There is a corresponding family of ODEs:

$$x'(t) = f(x(t), \lambda) \tag{44}$$

Suppose that $(x(\lambda), \lambda)$ is a branch of equilibria parametrized continuously by λ.

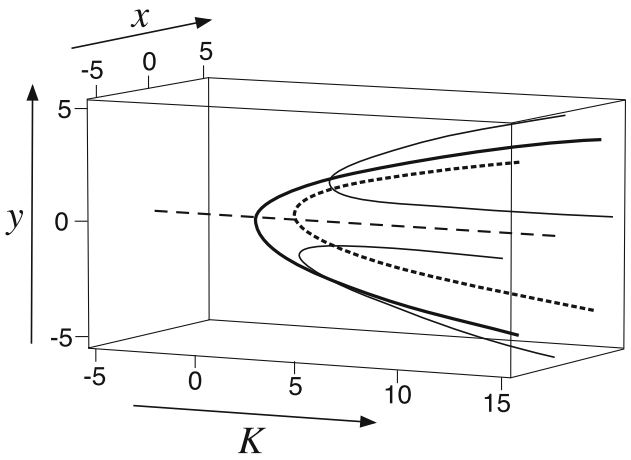

Fig. 3 Bifurcation diagram. Equation (32): *dashed*. Equations (33)/(36): *dotted*. Equations (34)/(37): *thick solid*. Equations (35)/(38)–(41): *thin solid*

A necessary condition for the occurrence of local bifurcation from some branch of equilibria is that the Jacobian $J = \mathrm{D}_x f|_{(x_0,\lambda_0)}$ should have eigenvalues on the imaginary axis (including 0). This is a consequence of the Implicit Function Theorem. A zero eigenvalue usually corresponds to steady-state bifurcation: typically, the number of equilibria changes near (x_0, λ_0), and branches of equilibria may appear, disappear, merge, or split. A nonzero imaginary eigenvalue usually corresponds to Hopf bifurcation: under suitable genericity conditions this leads to time-periodic solutions whose amplitude is small near the bifurcation point. In either case, the corresponding eigenspace E is said to be *critical*.

The basic existence theorem for bifurcating symmetry-breaking equilibria is the Equivariant Branching Lemma of Cicogna [13] and Vanderbauwhede [99]. Its statement requires the concept of an *axial* subgroup of Γ. This is an isotropy subgroup Σ for which

$$\dim \mathrm{Fix}(\Sigma) = 1 \tag{45}$$

in the action of Σ on E. The Equivariant Branching Lemma states that, subject to technical conditions [39,42] which are usually valid at a local steady-state bifurcation, for each axial subgroup $\Sigma \subseteq \Gamma$ there exists a branch of equilibria lying in $\mathrm{Fix}(\Sigma)$. This result guarantees the existence of bifurcating branches of solutions with symmetry at least Σ. Other branches may also occur: the axial condition is sufficient but not necessary for a branch to exist.

In Example 3.6, the Equivariant Branching Lemma predicts the existence of branches, bifurcating from the origin, for the isotropy subgroups $\{I, \sigma\}$ and $\{I, -\sigma\}$. The branches with trivial isotropy do not branch from the origin. See Table 3.

The basic general existence theorem for bifurcating symmetry-breaking periodic states runs along similar lines. The prototype is Hopf bifurcation. In the absence of symmetry, a Hopf bifurcation occurs when the critical eigenvalues are nonzero and

purely imaginary. Some technical conditions are also needed. When there is a non-zero imaginary critical eigenvalue, the corresponding eigenspace supports an action, not just of Γ, but of $\Gamma \times \mathbb{S}^1$ where $\mathbb{S}^1$ is the circle group. The $\mathbb{S}^1$-action is determined by the exponential of the Jacobian on the critical eigenspace E. If the imaginary eigenvalues are $\pm i\omega$, then $\theta \in \mathbb{S}^1$ acts on E like the matrix $\exp(\frac{2\pi\theta}{\omega} J|_E)$. The group $\mathbb{S}^1$ can be interpreted as phase shifts on time-periodic solutions.

The equivariant Hopf Theorem is analogous to the Equivariant Branching Lemma, but the symmetry group Γ is replaced by $\Gamma \times \mathbb{S}^1$. A subgroup $\Sigma \subset \Gamma \times \mathbb{S}^1$ is $\mathbb{C}$-*axial* if Σ is an isotropy subgroup of the action of $\Gamma \times \mathbb{S}^1$ on E and

$$\dim \mathrm{Fix}(\Sigma) = 2 \tag{46}$$

The Equivariant Hopf Theorem [39,42] states that, subject to technical hypotheses, if J has purely imaginary eigenvalues, then for any $\mathbb{C}$-axial subgroup $\Sigma \subset \Gamma \times \mathbb{S}^1$ there exists a branch of periodic solutions with spatio-temporal symmetry group Σ.

We apply the Equivariant Hopf Theorem to Example 3.5. The Jacobian at the origin is

$$J = \begin{pmatrix} -a & -1 & -c & 0 & 0 & 0 \\ b & -\gamma & 0 & 0 & 0 & 0 \\ 0 & 0 & -a & -1 & -c & 0 \\ 0 & 0 & b & -\gamma & 0 & 0 \\ -c & 0 & 0 & 0 & -a & -1 \\ 0 & 0 & 0 & 0 & b & -\gamma \end{pmatrix} \tag{47}$$

Its eigenvalues at parameters $a = b = \gamma = 0.5,\ c = 0.8$ are $-0.209 \pm 1.113i$, $-0.9 \pm 0.583i$, $-0.390 \pm 0.420i$, all with negative real part. Its eigenvalues at parameters $a = b = \gamma = 0.5\,,\ c = 2$ are $-2.207, -0.792, 0.401 \pm 1.943i, -0.401 \pm 0.211i$. Here one pair of complex conjugate eigenvalues has positive real part. The transition in which the real part becomes zero occurs near $c = 1.230$, at which the eigenvalues are $\pm 1.385i$, $-1.115 \pm 0.348i$, $-0.384 \pm 0.319i$. The critical eigenspace at $\pm 1.385i$ is spanned by

$$\begin{aligned} p = (&0.546, 0.063 - 0.174i, -0.273 - 0.473i, \\ &-0.182 + 0.032i, -0.273 + 0.473i, 0.119 + 0.141i) \end{aligned} \tag{48}$$

$$\begin{aligned} q = (&0.546, 0.063 + 0.174i, -0.273 + 0.473i, \\ &-0.182 - 0.032i, -0.273 - 0.473i, 0.119 - 0.141i) \end{aligned} \tag{49}$$

If $\omega = e^{2\pi i/3}$ then

$$\begin{aligned} \omega p = (&-0.273 + 0.473i, 0.119 + 0.141i, 0.546, \\ &0.063 - 0.174i, -0.273 - 0.473i, -0.182 + 0.032i) \end{aligned} \tag{50}$$

which is p with all entries shifted two spaces to the right, the effect of the 3-cycle (123). This shows the pattern of one-third period phase shifts.

4 Sympatric speciation

In *allopatric* speciation, phenotypic differences are triggered by environmental ones, and gene-flow is suppressed by a geographical barrier [73,82]. In *sympatric* speciation, the populations are not separated by a geographical barrier. Instead, the stabilizing effect of gene-flow is countered by some other factor, such as limited food resources, sexual selection, assortative mating, or environmental influences [22,48,57,63,83,87,95].

Until recently, the prevailing wisdom was that sympatric speciation is counterintuitive and rare, whereas allopatric speciation is straightforward and common. The main technical obstacle to sympatric speciation is gene-flow. If the two subpopulations representing nascent species coexist in the same habitat, they can interbreed; genetic differences between the two subpopulations will then be reduced as the two gene-pools are mixed together, restoring a single species. Sympatric speciation is also counterintuitive for evolutionary reasons: since both subpopulations are competing for the same resources, it is difficult to understand how their different survival strategies can make each of them "fitter" than the other. Equal fitness is biologically implausible and would be destroyed by small changes in the model.

These objections can be reinterpreted as informal symmetry arguments. Consider a population of nominally identical organisms, labelled $1, 2, \ldots, n$. Then our description of the population dynamics should not depend on which label we assign to each organism, so any plausible model should be equivariant under the action of the permutation group $\mathbb{S}_n$. Both arguments against sympatric speciation assume, tacitly, that this symmetry cannot break. The gene-flow argument provides the beginnings of a rationale for this assumption: the stabilizing effect of gene-flow should prevent symmetry-breaking. The evolutionary argument provides no such rationale. A number of recent studies, both theoretical and in the field, have examined these assumptions, not always explicitly, and observed that there are logical loopholes [22,48,57,63,83,95]. These studies challenge the intuition that sympatric speciation is rare or unusual. General properties of symmetry-breaking establish a number of phenomena likely to occur in any symmetry-breaking model [15,91,100]. Exact symmetry lacks biological realism; this can be restored by making the models stochastic, permitting phenotypic variability within a species. The same universal phenomena occur in stochastic symmetry-breaking models.

A population of organisms may be described by a probability density function $\Phi(x, t)$ where x is a vector of characters drawn from a phenotypic space X and t is time. If U is some region in X, then the probability of finding an organism with phenotype $u \in U$ is the integral

$$\int_{x \in U} \Phi(x, t)\, dx \tag{51}$$

A species corresponds to a relatively dense cluster in X. The dynamics of Φ determines how and when such clusters split. Discretize X into a finite number N of disjoint "bins" X_i [26,90], and model the dynamics by the system of ODEs

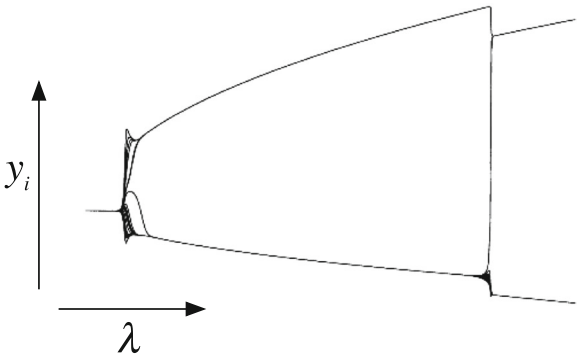

Fig. 4 Bifurcation diagram for sympatric speciation model. All y_i are plotted on the same vertical scale, with one curve for each $i = 1, \ldots, N$. Scales omitted because only the qualitative form is relevant here

$$x_i'(t) = f_i(x_1(t), \ldots, x_N(t)) \quad 1 \le i \le N \tag{52}$$

Here x_i represents the mean phenotype in bin X_i. The x_i are tokens for the phenotypic distribution [25], sometimes referred to as placeholders for organism dynamics (PODs). They provide a coarse-grained description of the distribution of phenotypes in the population, which is represented as an "ensemble" of tokens. The effect of environment, including other organisms, is incorporated by making Φ, hence the f_i, depend on one or more parameters λ. Similar models occur in adaptive dynamics [60], but usually in relation to genotype in heterogeneous environments, not phenotype in homogeneous ones.

As λ varies continuously, solutions of Eq. (52) may bifurcate [39]. Bifurcations introduce significant changes, in particular, a form of speciation, in which some tokens evolve different phenotypes from others. Broadly speaking, the main characteristic of a species is that the token phenotypes x_i are tightly clumped; in the simplest idealization they are identical. As all tokens then respond to each other in the same way, $f = (f_i)$ must be $\mathbb{S}_N$-equivariant.

The simplest symmetry-breaking bifurcation that can lead to stable steady states takes the form [15,25]

$$\begin{aligned} y_i'(t) = {} & \lambda y_i(t) + (N y_i(t)^2 - \pi_2(t)) + C(N y_i(t)^3 - \pi_3(t)) \\ & + D y_i(t) \pi_2(t) \quad (i = 1, 2, \ldots, N) \end{aligned} \tag{53}$$

where $\pi_2 = y_1^2 + \cdots + y_N^2$ and $\pi_3 = y_1^3 + \cdots + y_N^3$. Here λ, C, D are environmental parameters and λ drives the instability, hence the bifurcation. The y_i are the deviations of the original x_i from their mean, so the constraint $y_1 + \cdots + y_N = 0$ holds. Equation (53) has a gradient structure [21], so all dynamical trajectories converge to steady states.

A typical bifurcation diagram for equilibria is shown in Fig. 4, which depicts equilibria of Eq. (53) for fixed C, D as λ increases through 0. All y_i, $1 \le i \le N$ are plotted on the same vertical axis, and λ runs horizontally. Here a population with one phenotype bifurcates to a population with two distinct phenotypes. Within the assumptions of the model, the initial single species splits into two. Equivariant bifurcation theory for the group $\mathbb{S}_N$ implies that all such bifurcations share universal features [15,30]:

they are jumps, the mean phenotype remains approximately constant throughout the bifurcation, and the final state has two species. Exceptionally, three-species states may occur for short ranges of λ, but not stably [21]. Such states are produced by secondary bifurcations, such as the large jump visible towards the right of the figure.

The assumption that there is a symmetry-breaking bifurcation has a biological interpretation: it happens provided the unifying effect of gene-flow is outweighed by a sufficiently strong tendency towards diversity such as disruptive selection or assortative mating [82]. Associated genetic changes probably arise from recombination, not mutation. Because means are preserved, the bifurcation does not create significant changes in allele frequencies. Instead, the allele combinations in adults who survive to reproductive age change, with hybrids being eliminated or substantially reduced in frequency [15].

This kind of model has been placed on a more rigorous footing by using the POD variables x_i or y_i to define the phenotypic distribution as a weighted sum of translations of a fixed localized function, for example a Gaussian [26]. The weights are also permitted to vary dynamically.

5 Hallucination patterns

Geometric hallucination patterns can be induced in many ways, including flickering lights, pressure on the eyeballs, anesthetics, and hallucinogenic drugs; Fig. 5 shows some examples. Klüver [61] classified these patterns into four classes, which he named *form constants*: (I) gratings, lattices, fretworks, filigrees, honeycombs and checkerboards, (II) cobwebs, (III) tunnels, funnels, alleys, cones and vessels, and (IV) spirals.

The patterns arise in layer V1 of the visual cortex, but are interpreted by the visual system as if they had arisen in the eye. Their appearance to a subject therefore depends on the retino-cortical map, which transforms an image on the eye into an excitation pattern in the cortex. What is seen is the image of the cortical pattern under the inverse of this map. Ermentrout and Cowan [27] show that the map takes the form

$$x = \frac{\alpha}{\varepsilon}\log\left[1 + \frac{\varepsilon}{\omega_0} r_R\right] \quad y = \frac{\beta r_R \theta_R}{\omega_0 + \varepsilon r_R} \tag{54}$$

where (x, y) are cartesian coordinates on the cortex, (r_R, θ_R) are polar coordinates on the retina and $\omega_0, \varepsilon, \alpha, \beta$ are constants. The geometry of this logarithmic map is shown

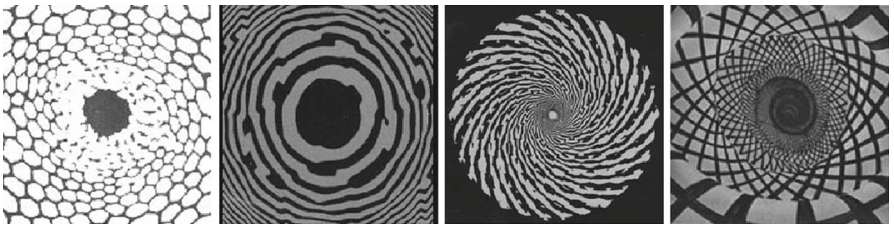

Fig. 5 Sample hallucination patterns. From *left to right* honeycomb, tunnel, spiral, lattice spiral. Courtesy of Bressloff et al.

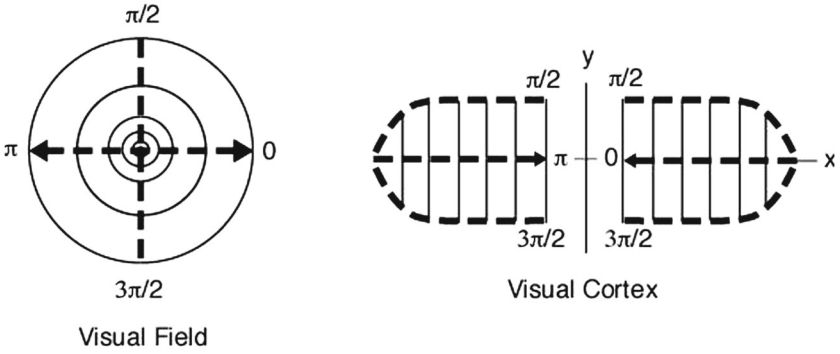

Fig. 6 Retino-cortical map. Courtesy of Bressloff et al.

in Fig. 6. Schwartz [86] suggested a mathematical explanation for the appearance of the complex logarithm in the transition from outside world patterns to V1 patterns. The density of neurons in the eye declines as $1/r^2$ from the fovea to the outer boundary, whereas V1 is a rectangle with constant neuron density. There is a unique density-preserving conformal map between these domains: the complex logarithm.

Ermentrout and Cowan [27] observed that circles and spirals on the retina correspond to parallel waves on the cortex, and modelled these in terms of interacting populations of excitatory and inhibitory neurons in a 2-dimensional layer. They modeled the evolution of the waves in terms of Wilson–Cowan equations [102,103], showing that spatially periodic patterns such as stripes can bifurcate from a homogeneous low-activity state via a Turing instability [96]. Their model also explains other patterns observed, by way of more complex Turing patterns. Cowan [18] interpreted the results in terms of symmetry-breaking, where the symmetry group is the Euclidean group $\mathbb{E}(2)$ of rigid motions of the plane.

Bressloff et al. [4] developed this model by taking into account experimental evidence about the neural connections in V1. This layer of the visual cortex comprises clusters of cells known as hypercolumns, which sense the direction in which images are oriented using local inhibitory connections and transmit this information to neighboring hypercolumns along the relevant direction via excitatory connections. Bressloff et al. [4] used a continuum model of V1 in which each point in the visual cortex has an associated circle of orientations, modeling a hypercolumn. The key point is that while the symmetry group of this model is also $\mathbb{E}(2)$, its action is different. Rotations in $\mathbb{E}(2)$ transform the plane, but they also induce rotations of the circular fiber above each point. This "shift-twist" action reflects the directional nature of the excitatory connections between nearby hypercolumns. They then used techniques of symmetric bifurcation theory to classify wave patterns in V1 (planforms) arising via steady-state bifurcations, triggered by the presumed action of hallucinogens or flickering lights. These patterns were then transformed via the inverse retino-cortical map to predict the resulting hallucination patterns. A special class of periodic states was also discussed, arising from a steady-state bifurcation with full circle group symmetry [38].

With the stated interpretation, the set of planforms generates representatives of all of Klüwer's form constants. The planforms naturally divide V1 into patches, in which the pattern has a near constant orientation. This is similar to the iso-orientation patches constructed via optical imaging of V1 activity. The boundaries of such regions correspond to the well-known 'pinwheels' [4]. They computed the stabilities of the patterns, verifying that stable patterns can account for the known form constants. The results are sensitive to the specification of the lateral connectivity, and suggest that the cortical mechanisms generating geometric visual hallucinations may be closely related to those involved in the processing of edges and contours.

6 Hyperbolic tilings and neuroscience

With the above work as a starting-point, Chossat and Faugeras [10] have analyzed a model for the visual perception of textures, which leads to a formulation in terms of symmetry groups of tilings in the hyperbolic plane. The hyperbolic plane arises in non-Euclidean geometry, and can be thought of as geometry on a surface of constant negative curvature. Chossat and Faugeras work in the Poincaré disk model of the hyperbolic plane. As a subset of the standard Euclidean plane, this model represents the hyperbolic plane as the interior of the unit disk, with a metric in which geodesics are arcs of circles that meet the boundary circle at right angles. Only the parts of these circles that lie in the interior of the unit disk are considered. Hyperbolic geometry has a long classical history, see for example Greenberg [44].

The idea is further developed by Chossat et al. [11] and by Faye and Chossat [28]. The Poincaré disk arises from the proposal that populations of neurons in each hypercolumn of V1 detect information about the structure tensor of the image. This is a 2×2 positive definite symmetric matrix whose eigenvalues and eigenvectors characterize various geometric features of the image, such as the presence and orientation of edges and the amount of contrast. The average membrane potential V of the population of neurons in a hypercolumn can be expressed as a function of the structure tensor and time. It is then possible to write down an integro-differential equation for the time evolution of the structure tensor. On the assumption that this equation is symmetric—invariant under the isometries of the appropriate space—the bifurcations of the structure tensor are determined by an equivariant bifurcation problem on the hyperbolic plane, which naturally arises here as the Poincaré disk.

The symmetry group of the hyperbolic plane, the group of rigid hyperbolic motions, analogous to the Euclidean group $\mathbb{E}(2)$, is non-compact, and this causes technical difficulties, for example with regard to irreducible representations. To obtain a compact Lie group action, the paper restricts attention to patterns that repeat on the hyperbolic analogue of a periodic lattice. Such patterns can be thought of as repetitive tilings, using images of a fixed tile under hyperbolic rigid motions. Typically the tiles are regular polygons, and in a Euclidean view of the unit disk they have curved sides.

This assumption is similar to the assumption of a periodic lattice in the Euclidean plane in the previous section. It reduces the problem to bifurcation on a compact Riemann surface. The bifurcating patterns are called H-planforms, by analogy with the Euclidean case. The Equivariant Branching Lemma is then used to prove the existence

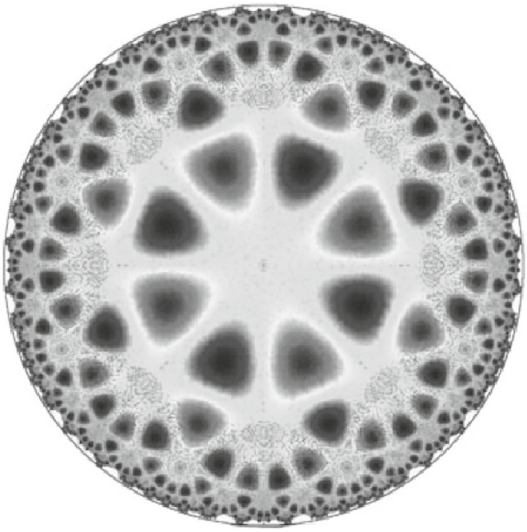

Fig. 7 Pattern in the hyperbolic plane, realized in the Poincaré disk model, based on a tiling by octagons. Courtesy of Chossat

of certain bifurcating branches of patterns for the simplest hyperbolic lattice, consisting of tilings by a regular octagon. The symmetry group of the bifurcation problem on the Riemann surface has order 96. Figure 7 shows one of the resulting patterns.

The suggested biological interpretation of these results leads to two lines of investigation. Because of the connection with structure tensors, H-planforms may be involved in the process of defining texture tuning curves, in a manner that is analogous to the role in planforms in orientation selectivity in Bressloff et al. [4]. The second is that H-planforms may be related to neural illusions caused by the coexistence of several stable equilibria of the evolution equation.

7 Animal Locomotion

There are regular patterns in the movements of animals [1,43]. These patterns are called *gaits*, and many gaits are symmetric. Methods from equivariant dynamics have been used [5,6,16,17,40,41] to classify these symmetries and to deduce the simplest architecture for a central pattern generator (CPG), a relatively simple network of neurons that is thought to generate the gait rhythms [64,65].

The patterns in legged locomotion are spatio-temporal symmetries. The spatial symmetries are permutations of the legs, so the gaits are invariant under certain permutations of the legs, combined with a temporal phase shift. Figure 8 illustrates some common gait patterns; the four lines represent legs and the numbers are the corresponding phase shifts. Informally, the legs move periodically in specific sequences with specific time delays, expressed as a fraction of the overall period. For example, in the *trot* of a horse, diagonally opposite legs move together, the two diagonals being half a period out of phase. In the *walk*, successive legs hit the ground at intervals of one quarter period, in the order: left rear, left front, right rear, right front. The left/right mirror image of this pattern can also occur. In the *pace*, common in the camel and

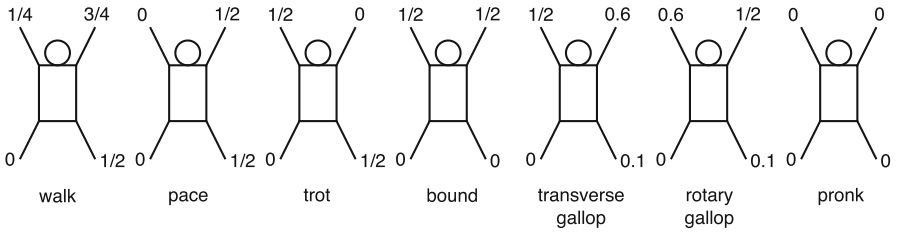

Fig. 8 Seven common quadrupedal gaits. *Numbers* indicate the percentage of the time through the gait when the associated leg first strikes the ground. By convention, gaits begin when the left hind leg strikes the ground. Animal viewed from above

giraffe paces, both left legs move together, then both right legs, half a period out of phase. In the *bound*, common in dogs and rabbits, the back legs move together, then the front legs, again half a period out of phase. In the most symmetric gait of all, the *pronk*, all four legs hit the ground simultaneously. This gait is found in deer, gazelles, and many young animals. Highly symmetric gaits such as these are called *primary* gaits.

There are also more complex gaits, such as the *transverse gallop* of the horse and the *rotary gallop* of the cheetah, with phase shifts that are not such simple fractions of the period. Such gaits are called *secondary* gaits.

The existence of a CPG is supported by a substantial amount of indirect evidence [46], but significant information on the detailed structure of the CPG is known only for a few animals, notably the lamprey [45]. For most animals, even the existence of a CPG has not been confirmed directly, though it is well established that the basic rhythms of locomotion are generated somewhere in the spinal cord, not in the brain. The symmetry approach provides a rationale for gait patterns and illuminates the distinction between primary and secondary gaits. It suggests a schematic form of the animal's CPG.

The starting point for this inference is the phase shifts. It can be proved, in a fairly general context, that whenever specific phase shifts occur in a robust manner in some network, with the oscillations concerned being otherwise identical, then the network has a cyclic group symmetry [35,36,92,93]. Any generator of this group corresponds to a phase shift of $\frac{kT}{n}$, where T is the overall period, n is the order of the cyclic group, and $0 \leq k \leq n-1$. In quadruped locomotion, the phase shifts occurring in the most symmetric gaits are all integer multiples of $\frac{T}{4}$, suggesting that the symmetry group should include $\mathbb{Z}_4$. Since the most realistic symmetry of the animal is left/right mirror symmetry, it is also reasonable to assume that the CPG has this symmetry. Moreover, there are reasons to expect that the mirror symmetry should not be included in the $\mathbb{Z}_4$ symmetry group. Informally, the most plausible symmetry group for the CPG of a quadruped should be $\mathbb{Z}_2 \times \mathbb{Z}_4$. Schematically, the associated architecture should resemble Fig. 9, with 8 nodes. Each leg is controlled by signals from two nodes, which affect different muscle groups: once causes the leg to flex, the other causes it to extend.

This diagram is schematic. Each node might represent a subnetwork of neurons, with the same subnetwork in each node. The connections indicate the overall symmetry, and do not imply that only the links shown occur. Any node might be connected to

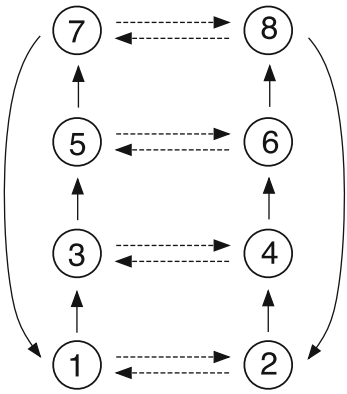

Fig. 9 Eight-cell network for quadrupeds. *Dashed lines* indicate contralateral coupling; *single lines* indicate ipsilateral coupling

Table 5 Phase shifts for primary gaits in the eight-cell network

Legs		Walk	Jump	Trot	Pace	Bound	Pronk
L front	R front	$\frac{3}{4}$ $\frac{1}{4}$	$\frac{1}{2}$ $\frac{1}{2}$	$\frac{1}{2}$ 0	0 $\frac{1}{2}$	$\frac{1}{2}$ $\frac{1}{2}$	0 0
L rear	R rear	$\frac{1}{2}$ 0	$\frac{3}{4}$ $\frac{3}{4}$	0 $\frac{1}{2}$	0 $\frac{1}{2}$	0 0	0 0
L front	R front	$\frac{1}{4}$ $\frac{3}{4}$	0 0	$\frac{1}{2}$ 0	0 $\frac{1}{2}$	$\frac{1}{2}$ $\frac{1}{2}$	0 0
L rear	R rear	0 $\frac{1}{2}$	$\frac{1}{4}$ $\frac{1}{4}$	0 $\frac{1}{2}$	0 $\frac{1}{2}$	0 0	0 0
Subgroup K		$\mathbb{Z}_2(\kappa\omega^2)$	$\mathbb{Z}_2(\kappa)$	$\mathbb{Z}_4(\kappa\omega)$	$\mathbb{Z}_4(\omega)$	$\mathbb{D}_2(\kappa, \omega^2)$	$\mathbb{Z}_2 \times \mathbb{Z}_4$

any other; however, such connections should occur in symmetrically related sets of 8 or 4 links. In Golubitsky et al. [40,41] and Buono and Golubitsky [6], this architecture is deduced from an explicit list of assumptions, and is proved to be unique. A 4-node network is not suitable, because in a 4-node network trot and pace are forced to coexist and have the same stabilities for any animal that can walk. This conflicts with observations: most horses walk and trot but do not pace; camels and giraffes walk and pace but do not trot. For dogs, the stabilities of pace and trot are different [2].

Buono and Golubitsky [6] apply the H/K theorem to predict that for suitable dynamics of nodes and connections, the network in Fig. 9 typically generates a range of symmetric patterns of oscillation; see Table 5. Primary states are characterized by all eight cells having the same waveform modulo phase shift, that is, $H = \Gamma$. Secondary gaits involve more than one waveform: $H \subsetneq \Gamma$. The six subgroups $K \subset H$ for which H/K is cyclic determine the primary patterns for the 8-cell network, shown in Table 5. There is an analogous but more complicated classification of secondary gaits [5].

The patterns in Table 5 correspond to standard primary quadruped gaits, except for "jump". The jump gait was observed at the Houston Livestock Show and Rodeo. Figure 10 shows four video frames of a bucking bronco, taken at equal intervals of time. The interval between the footfalls is very close to $\frac{1}{4}$ of the period. The primitive ricocheting jump of the Norway rat and Asia Minor gerbil also has this pattern of phases [33].

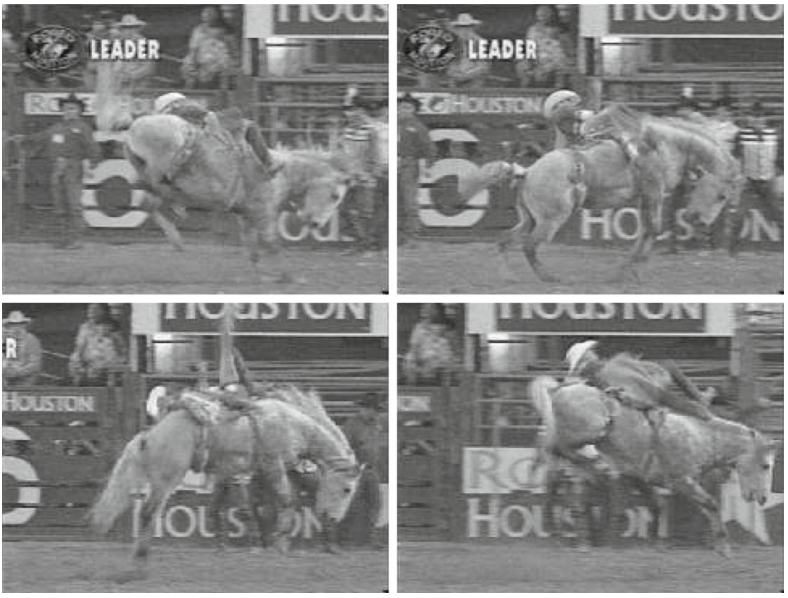

Fig. 10 Quarter cycles of bareback bronco jump at Houston Livestock Show and Rodeo. *Top left* fore legs hit ground. *Top right* hind legs hit ground. *Bottom left and right* all legs in air

The equivariant Hopf theorem has been used to classify natural oscillations in the sensory system in the ears that controls balance—the vestibular system. McCollum and Boyle [74] observed that in the cat the network of neurons concerned possesses octahedral symmetry, a structure that they deduce from the known innervation patterns (connections) from canals to muscles. Golubitsky et al. [37] derive octahedral symmetry from network architecture, and model the movement of the head in response to activation patterns of the muscles.

8 Pattern formation in animal markings and form

Organisms often exhibit patterns of form or markings, and many of these patterns have symmetry. Turing [96] modeled these patterns in terms of a system of reaction–diffusion equations:

$$\partial q/\partial t = D\nabla^2(q(x,t)) + F(q(x,t)) \tag{55}$$

defined on a domain Ω. Here $q(x,t)$ is a time-varying pattern of concentrations of a system of molecules, called a *morphogen*, for $x \in \Omega$, $t \in \mathbb{R}$. The function F represents reaction kinetics. The pattern of concentrations q is interpreted as a genetic prepattern in the organism. This pattern is created by the dynamics of F in conjunction with diffusion, defined by the term $D\nabla^2(q(x,t))$, with D a matrix of diffusion coefficients. As the organism develops, the prepattern is expressed either as a corresponding change in form, or as a pattern of visible markings produced by pigment proteins.

Common domains Ω include a line, a circle, a plane, a torus, a sphere, or the whole of $\mathbb{R}^3$. These domains have nontrivial symmetries, which induce symmetries in bifurcation equations. Spontaneous symmetry-breaking leads to patterns whose symmetries correspond to some subgroup of this symmetry group. In some cases, in particular when the problem is posed with Neumann boundary conditions, the equations may have more symmetry than the domain. These extra symmetries are translations of the domain that leave it invariant after a cut-and-paste construction et al. [20].

Similar remarks apply to generalizations of Eq. (55), which model a wide range of biological pattern formation [79]. If q is 1-dimensional and Ω is a circle, $D \in \mathbb{R}$ is a scalar and the symmetries of the domain are rotations and reflections of the circle, the group $\mathbb{O}(2)$. Use an angle $\theta \in [0, 2\pi)$ as a coordinate on the domain, replacing x above. Suppose there exists an equilibrium state $q(\theta, t) \equiv q_0$, so that $F(q_0) = 0$. Change coordinates from q to $q - q_0$, so that $F(0) = 0$. We can use equivariant bifurcation theory to investigate symmetry-breaking equilibrium patterns. A similar analysis using Hopf bifurcation yields time-periodic patterns. In the equilibrium case, the linearization of Eq. (55) at the origin is

$$0 = Dq''(\theta) + F_0 q(\theta) \tag{56}$$

where $F_0 = F'(0)$. We rewrite this as

$$q''(\theta) + k^2 q(\theta) = 0 \tag{57}$$

where $k^2 = F_0/D$. The general solution of Eq. (57) is

$$q(\theta) = a \cos k\theta + b \sin k\theta \tag{58}$$

leading to patterns with k-fold rotational symmetry. To find out when these patterns survive the addition of the nonlinear terms, we use the symmetry explicitly. The group $\mathbb{O}(2)$ acts on the space of all real-valued functions on the circle. This space splits into "irreducible" components: subspaces invariant under the group action that contain no subspaces with that property except themselves and zero. Here the irreducible components V_k are precisely the spaces of functions given by Eq. (58) for integer $k \geq 0$. Each V_k is 2-dimensional, except for V_0 which is 1-dimensional because $\sin 0 = 0$.

For $k > 0$ the action of $\mathbb{O}(2)$ on V_k is induced from the action on θ given by:

$$R_\phi(\theta) = \theta + k\phi \qquad \kappa(\theta) = -\theta \tag{59}$$

The subgroup $\mathbb{Z}_k\langle \frac{2\pi}{k} \rangle$ acts trivially. The only nontrivial isotropy subgroup is generated by $\mathbb{Z}_k\langle \frac{2\pi}{k} \rangle$ together with $\mathbb{Z}_2\langle \kappa \rangle$. This is a dihedral group $\mathbb{D}_k$. The Equivariant Branching Lemma implies that generically there will be a symmetry-breaking branch of equilibria with $\mathbb{D}_k$ symmetry. The profile of q will be close to that of the linearized eigenfunction $a \cos k\theta$.

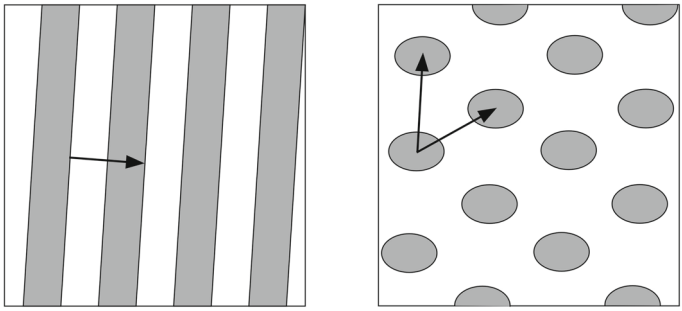

Fig. 11 *Left* Stripes. *Arrow* shows v_0. *Right* Spots. *Arrows* show v_0, w_0

Dihedral group symmetries are common in the animal and plant kingdom. Turing [96] proposed that the tentacles of *Hydra* might be generated by symmetric equilibria of this kind. Many chinoderms have symmetry $\mathbb{D}_5$; some have symmetries $\mathbb{D}_k$ with $k > 5$. The eleven-armed sea star *Coscinasterias calamaria* found around southern Australia and New Zealand has symmetry $\mathbb{D}_{11}$. Solasteridae typically have 10–15 arms, and the Antarctic *Labidiaster annulatus* can have up to 50.

Markings on animals, such as spots and stripes, can be modeled using a planar domain $\Omega = \mathbb{R}^2$ or a cylindrical domain. The patterns that arise can be classified using the symmetries of the domain. In many cases their existence in the nonlinear model is a consequence of the Equivariant Branching Lemma. For a planar domain the symmetry group is the Euclidean group $\mathbb{E}(2)$. The simplest isotropy subgroups are the group $\mathbb{Z}\langle v_0\rangle$ of translations by integer multiples of a constant vector $v_0 \neq 0$, and the group $\mathbb{Z}\langle v_0, w_0\rangle$ of translations by integer linear combinations $av_0 + bw_0$ of two linearly independent vectors v_0, w_0. The corresponding patterns are parallel *stripes* at right angles to v_0 and distance $||v_0||$ apart, and a lattice of *spots* repeating when translated by v_0 or w_0; see Fig. 11.

When the domain is a disk in the plane, the linearized eigenfunctions are Bessel functions of the radius multiplied by trigonometric functions of the angle. Among the time-periodic patterns predicted by symmetry are rotating spirals and expanding target patterns [34]. These patterns are found in the Belousov–Zhabotinskii reaction: Fig. 12 shows numerically computed patterns for a model of Fitzhugh–Nagumo type [3]. The equations are

$$\begin{aligned} \partial u/\partial t &= d_u^2 \Delta u(t) + \lambda u(t) - u(t)^3 - \sigma v(t) + \kappa, \\ \tau \partial v/\partial t &= d_v^2 \Delta v(t) + u(t) - v(t) \end{aligned} \tag{60}$$

For the spiral pattern, parameter values are $\lambda = 4.67, \tau = 4.0, d_u^2 = 0.0015, d_v^2 = 0.01, \kappa = -1.126, \sigma = -3.33$. For the target pattern, they are $\lambda = 0.9, \tau = 4.0, d_u^2 = 0.000964, d_v^2 = 0.0001, \kappa = 0, \sigma = 1$.

Similar patterns in slime molds have been modeled using a generalization of reaction–diffusion equations which relates the motion of slime-mold amoebas to cAMP signaling [50]. In the normal human heartbeat, electrical pacemaker waves propagate through the heart muscles like target patterns, and spiral waves, often occurring as many spirals forming "spiral chaos", can be fatal [66,67,104].

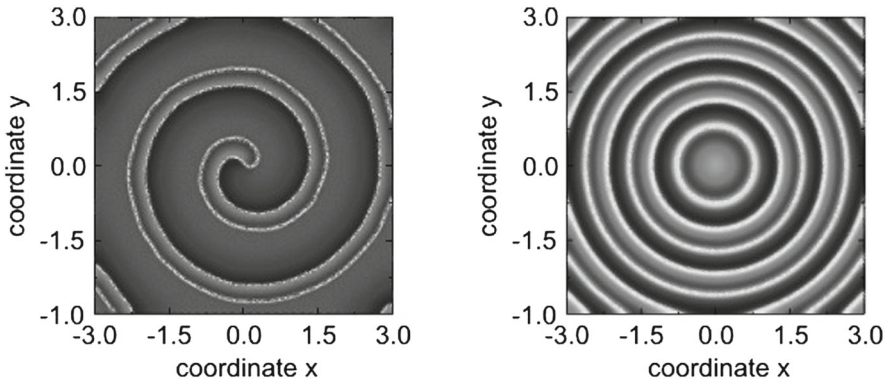

Fig. 12 Belousov–Zhabotinskii reaction. *Left* Spirals. *Right* Target patterns. Courtesy of Bödeker [3]

If the domain is a sphere or hemisphere, the linearized eigenfunctions are spherical harmonics. Nagata et al. [80] use symmetric bifurcation theory to study reaction–diffusion equations on a hemisphere, modeling pattern formation at the tip of a growing plant. McNally and Cox [75] use spherical harmonics to predict patterns for the slime mold *Polysphondylium pallidium*, which forms spherical masses. In normal morphogenesis this mass develops tips at equidistant points on the equator, but nowhere else. The paper studies new abnormal patterns distributed over the surface of the sphere.

In developmental biology, Turing's model proved controversial, in part because it did not identify specific morphogens and ignored the role of genetics. It was supplanted by the theory of positional information [105], in which chemical gradients correlated with the position of a cell cause particular genes to be expressed. Tissue transplant experiments, especially on the development of digits in chick and mouse embryos, appeared to favor this theory. However, the Turing model is currently experiencing a revival, as more biochemical details become available. Kondo and Asai [62] observe that patterns of stripes on the marine angelfish *Pomacanthus* change as the fish develops, and show that simulations using a Turing model correctly predict future patterns. They state that "the striking similarity between the actual and simulated pattern rearrangement strongly suggests that a reaction–diffusion wave is a viable mechanism". Sheth et al. [88] report transplant experiments in mice involving a larger number of digits than those studied previously, and show that as the effect of a particular set of genes decreases, the mouse grows more digits. These results are incompatible with the theory of positional information, but are predicted by a Turing model: the number of digits is determined by the number of waves occurring in the domain. Sick et al. [89] show that the spacing of hair follicles in mice is controlled by a reaction–diffusion mechanism in which the morphogens are the biochemical signalling system WNT and proteins in the DKK family which inhibit WNT. Economou et al. [24] show that ridge patterns inside a mouse's mouth are controlled by a Turing process.

9 Central place theory in geography

Ikeda et al. [53–55] apply pattern formation on a lattice to model how economic factors affect the geographical distribution of humans into cities.

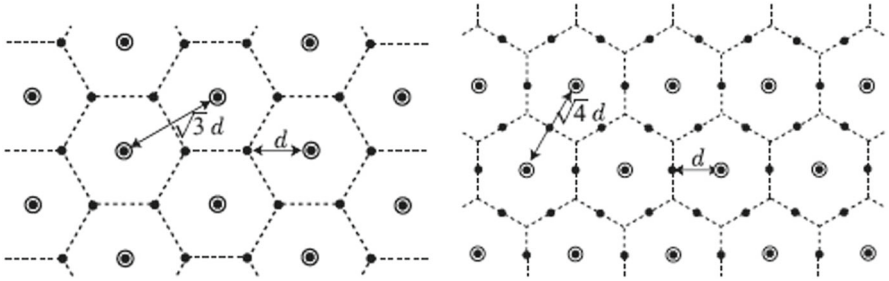

Fig. 13 Two of Christaller's patterns. *Dots* are population clusters, and the *size of the dot* indicates the population size. Courtesy of Ikeda

Lösch [71] proposed ten distinct hexagonal configurations as fundamental sizes for market areas. Christaller [12] developed a model of market areas based on economic, logistical, and administrative principles. This led to a hexagonal lattice with primary markets ("cities") at the centre of each hexagon, and to more elaborate arrangements, also on a hexagonal lattice, a proposal known as central place theory; see Fig. 13. Hexagons arise because "close-packed" configurations tend to be optimal. More generally, market areas of different scales can form a hierarchical arrangement of hexagons of different sizes.

The models of Lösch [71] and Christaller [12] are phenomenological: not derived from standard economic principles of market equilibrium. Clarke and Wilson [14] and Munz and Weidlich [78] addressed this deficiency. Krugman [68] showed that the hexagonal distributions of central place theory can be self-organized in core-periphery models, which describe population migration among cities, driven by microeconomics.

Ikeda et al. [55] derive Lösch's ten hexagonal lattice patterns by applying the Equivariant Branching Lemma to a core-periphery model in the plane. The symmetry-based techniques go back to Sattinger [84] and the singularity-theoretic approach of Buzano and Golubitsky [8], who analyzed a physical system that also forms hexagonal patterns: Bénard convection, in which a flat layer of fluid is heated from below. The homogeneous state loses stability, triggering a symmetry-breaking bifurcation to a doubly periodic tiling by hexagons. Ikeda et al. [55] discretize the spatial structure, employing a hexagonal lattice with periodic boundaries, formed from $n \times n$ uniformly distributed places connected by roads of the same length, forming a mesh of equilateral triangles. They formulate microeconomic interactions and worker migration using a core-periphery model. The symmetry group is a semidirect product $\mathbb{D}_6 \dot{+} (\mathbb{Z}_n \times \mathbb{Z}_n)$. This is analogous to the symmetry group analyzed in Buzano and Golubitsky [8], except that this paper uses a continuous symmetry group, the torus $\mathbb{S}^1 \times \mathbb{S}^1$, instead of $\mathbb{Z}_n \times \mathbb{Z}_n$.

Ikeda et al. [55] classify the axial subgroups of this symmetry group and apply the Equivariant Branching Lemma to characterize the isotropy subgroups of possible equilibria. They use numerical methods to determine which of these solutions occur in their model. Figure 14 shows two sample patterns that are demonstrated to occur. On the left is one of Christaller's patterns; on the right is a complicated pattern corresponding to "super-hexagon" states in Bénard convection found by Kirchgässner [59] and Dionne et al. [23].

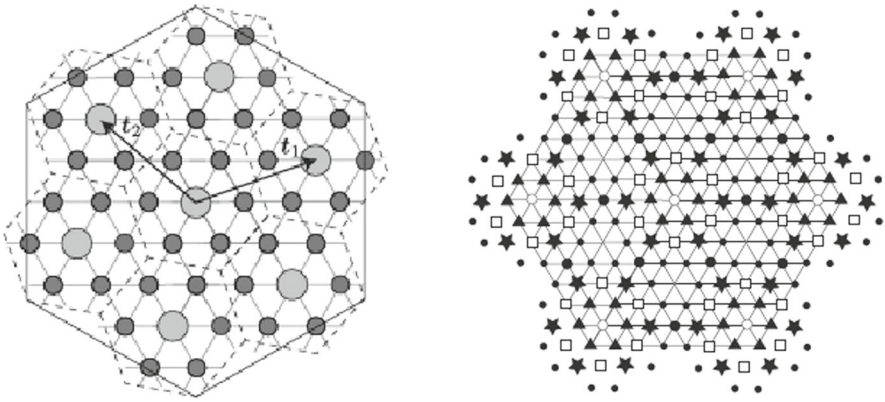

Fig. 14 *Left* One of Christaller's patterns, derived from a core-periphery model. *Right* A superhexagon pattern

All ten of Lösch's hexagonal distributions are proved to exist, as a consequence of the Equivariant Branching Lemma and numerical analysis. The paper provides a "missing link" between central place theory and economic geography. Similar models might be applied to pattern-formation in ecosystems, exploiting analogies between ecology and economics.

10 Virus structure

Symmetry methods can be used in a direct geometric manner, rather than through the intermediary of nonlinear dynamics and bifurcation theory. The main technique is representation theory, which classifies how a given abstract group can act as linear transformations of a vector space. The same group can act on spaces of several different dimensions. Such actions are of practical importance even if the dimension of the space is greater than three; for example, it might be a space of Fourier modes, representing spatial or temporal patterns, and the space of possible patterns may have high dimension even if the patterns themselves are viewed in $\mathbb{R}^2$ or $\mathbb{R}^3$.

The majority of viruses are either icosahedral (Fig. 15) or helical. Virus capsids—their external coats—are typically constructed from many copies of a roughly spherical protein molecule called a capsomer. A collection of molecules has the least energy when it is as close as possible to a sphere. Among the regular solids, the icosahedron is closest to a sphere; the truncated icosahedron, which is not regular but has the same symmetry group, is even closer to a sphere, and it provides an overall mathematical "skeleton" for many icosahedral viruses. Regular solids are highly symmetric; the dodecahedron and icosahedron have 120 symmetries, and so do their truncations.

Capsomers are either hexamers, surrounded by six others, or pentamers, surrounded by five others. In such cases there is a topological constraint on the number of pentamers. Euler's formula [19] states that for any polyhedron topologically equivalent to a sphere,

$$F - E + V = 2 \tag{61}$$

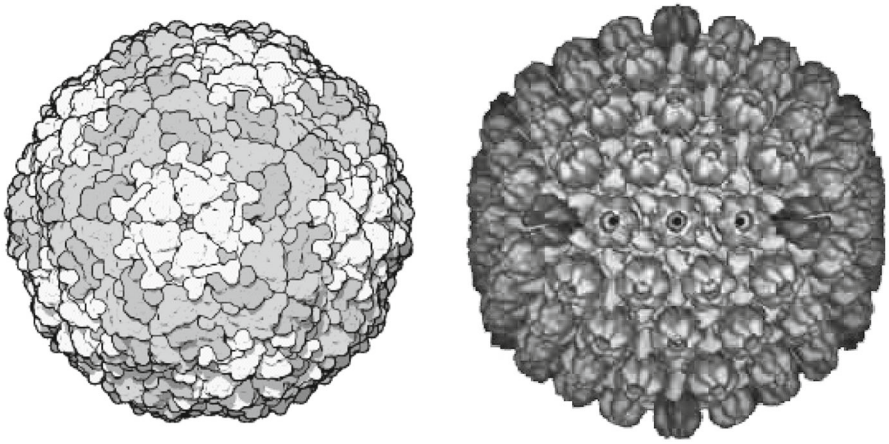

Fig. 15 Icosahedral structure of two viruses. *Left* Foot-and-mouth disease virus differs from its mirror image and has 60 symmetries. *Right Herpes simplex* virus is very close to mirror-symmetric and has 120 symmetries

where F is the number of faces, E the number of edges and V the number of vertices. Equation (61) implies that there must be exactly 12 pentamers in any virus coating composed solely of hexamers and pentamers.

Caspar and Klug [9] considered both helical and icosahedral viruses. In the icosahedral case they analyzed configurations in which each capsomer is surrounded by exactly the same configuration of adjacent units. This condition implies a high degree of symmetry, and immediately suggests the regular solids. The icosahedron is especially plausible because it is the best approximation to a sphere, and is therefore either an energy minimum or close to one. (Caspar and Klug also emphasized that the observed form of the capsid need not imply that the symmetry is icosahedral at a molecular level.) This symmetry condition implies that the number of capsomers is 12, 20 or 60. However, no known viruses employed these numbers, and most had more than 60 capsomers. None had a multiple of 60 units, which might be realized by relaxing the symmetry requirement slightly. Caspar and Klug therefore relaxed the symmetry requirement even further, which led them to shapes like the geodesic domes of the architect Buckminster Fuller, formed from triangles that are approximately equilateral [76]. Such arrangements do not have perfect symmetry; instead, triangles have two different kinds of neighborhood. Equation (61) implies that some must be arranged five to a vertex, while the rest fit six to a vertex. Caspar and Klug suggested using pseudo-icosahedra, solids that can be constructed from a tiling of the plane by equilateral triangles; see Fig. 16. First, choose two integers a and b. Starting from a vertex, move a units to the right and b units at 120° to get a second vertex. Place the third vertex to form a large equilateral triangle containing many vertices of the original tiling. Twenty large triangles fit together to form an icosahedral polyhedron with $10(a^2 + ab + b^2) + 2$ vertices, of which 12 are pentamers and the rest hexamers. The pentamers always lie on the axes of icosahedral symmetry.

The Caspar–Klug theory applies to many icosahedral viruses, but there are exceptions. Wrigley [106,107] observed icosahedral viruses that are not pseudo-icosahedral.

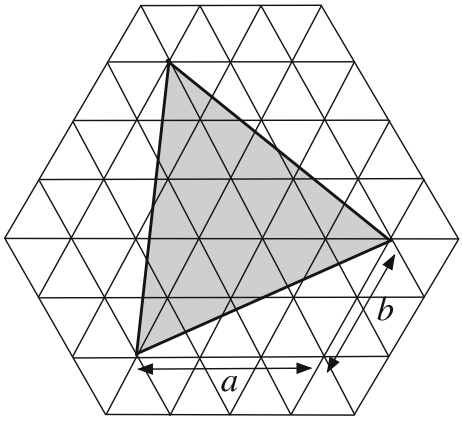

Fig. 16 Constructing one of the 20 faces of a pseudo-icosahedron

Instead, they can be described by Goldberg polyhedra, hexagonal packings on the surface of an icosahedron. Liddington et al. [70] discovered that polyoma virus has many more pentamers than the 12 found in pseudo-icosahedra and Goldberg polyhedra.

To explain these structures, Twarock [97,98] developed a more general theory of virus geometry, based on symmetry principles closely analogous to the group theory of the icosahedron. Their analysis, known as viral tiling theory, leads to geometry in six dimensions, not three. In viral tiling theory, pentamers need not lie on the symmetry axes of the underlying icosahedron. Higher-dimensional representations of the icosahedral group provide regular patterns, suitable sections of which can be projected into three dimensions to produce complex arrangements related to the icosahedron and its symmetries. Representation theory of the icosahedral group shows that the smallest dimension of a lattice with icosahedral symmetry is 6.

The icosahedral group belongs to an important class of symmetry groups known as Coxeter groups [52]. Keef and Twarock [58] apply this class of groups to the structure of icosahedral viruses in terms of a lattice D_6 in $\mathbb{R}^6$ with icosahedral symmetry. They construct a class of possible virus structures defined as projections from this lattice into $\mathbb{R}^3$. This technique yields all pseudo-icosahedra, together with structures that have more than 12 pentamers. Viral tiling theory accounts in particular for the structures of polyoma virus, Simian virus 40, and bacteriophage HK97.

The resulting structures have biological and potential medical interest because one way to attack a virus is to interfere with its assembly process. The geometry of the virus provides clues about potential weak points. Viral tiling theory also opens up new ways of thinking about tubular malformations, where the virus assembles into a tube rather than an approximate sphere. Understanding these errors might make it possible to interfere with virus replication.

References

1. Alexander, RMcN, Goldspink, J.M. (eds.): Mechanics and Energetics of Animal Locomotion. Chapman and Hall, London (1977)
2. Blaszczyk, J., Dobrzecka, C.: Alteration in the pattern of locomotion following a partial movement restraint in puppies. Acta Neurobiol. Exp. **49**, 39–46 (1989)

3. Bödeker, H.U.:http://en.wikipedia.org/wiki/Reaction%E2%80%93diffusion_system
4. Bressloff, P.C., Cowan, J.D., Golubitsky, M., Thomas, P.J., Wiener, M.C.: Geometric visual hallucinations, Euclidean symmetry, and the functional architecture of striate cortex. Philos. Trans. R. Soc. (Lond.) B **356**, 1–32 (2001)
5. Buono, P.-L.: Models of central pattern generators for quadruped locomotion. II. Secondary gaits. J. Math. Biol. **42**, 327–346 (2001)
6. Buono, P.L., Golubitsky, M.: Models of central pattern generators for quadruped locomotion: I. Primary gaits. J. Math. Biol. **42**, 291–326 (2001)
7. Buono, P.-L., Lamb, J.S.W., Roberts, R.M.: Bifurcation and branching of equilibria in reversible equivariant vector fields. Nonlinearity **21**, 625–660 (2008)
8. Buzano, E., Golubitsky, M.: Bifurcation on the hexagonal lattice and the planar Bénard problem. Philos. Trans. R. Soc. Lond. A **308**, 617–667 (1983)
9. Caspar, D.L.D., Klug, A.: Physical principles in the construction of regular viruses. In: Cold Spring Harbor Symposia on Quantitative Biology, vol. 27, pp. 1–24. Cold Spring Harbor Laboratory, New York (1962)
10. Chossat, P., Faugeras, O.: Hyperbolic planforms in relation to visual edges and textures perception. PLoS Comput. Biol. **5**(12), e1000625 (2009)
11. Chossat, P., Faye, G., Faugeras, O.: Bifurcation of hyperbolic planforms. J. Nonlinear Sci. **21**(4) (2011). doi:10.1007/s00332-010-9089-3
12. Christaller, W.: Central Places in Southern Germany. Prentice Hall, Englewood Cliffs (1966)
13. Cicogna, G.: Symmetry breakdown from bifurcations. Lett. Nuovo Cimento **31**, 600–602 (1981)
14. Clarke, M., Wilson, A.G.: The dynamics of urban spatial structure: the progress of a research programme. Trans. Inst. Br. Geogr. **10**, 427–451 (1985)
15. Cohen, J., Stewart, I.: Polymorphism viewed as phenotypic symmetry-breaking. In: Malik, S.K. (ed.) Nonlinear Phenomena in Physical and Biological Sciences, pp. 1–63. Indian National Science Academy, New Delhi (2000)
16. Collins, J.J., Stewart, I.: Hexapodal gaits and coupled nonlinear oscillator models. Biol. Cybern. **68**, 287–298 (1993)
17. Collins, J.J., Stewart, I.: Coupled nonlinear oscillators and the symmetries of animal gaits. J. Nonlinear Sci. **3**, 349–392 (1993)
18. Cowan, J.: Spontaneous symmetry beaking in large scale nervous activity. Int. J. Quantum Chem. **22**, 1059–1082 (1984)
19. Coxeter, H.S.M.: Introduction to Geometry. Wiley, New York (1961)
20. Crawford, J.D., Golubitsky, M., Gomes, M.G.M., Knobloch, E., Stewart, I.: Boundary conditions as symmetry constraints. In: Roberts, R.M., Stewart, I. (eds.) Singularity Theory and its Applications—Warwick 1989, Part II: Singularities, Bifurcations and Dynamics, Lecture Notes in Mathematics, vol. 1463, pp. 63–79. Springer, Heidelberg (1991)
21. Dias, A.P.S., Stewart, I.: Secondary bifurcations in systems with all-to-all coupling. Proc. R. Soc. Lond. A **459**, 1–18 (2003)
22. Dieckmann, U., Doebeli, M.: On the origin of species by sympatric speciation. Nature **400**, 354–457 (1999)
23. Dionne, B., Silber, M., Skeldon, A.C.: Stability results for steady, spatially periodic planforms. Nonlinearity **10**, 321–353 (1997)
24. Economou, A.D., Ohazama, A., Porntaveetus, T., Sharpe, P.T., Kondo, S., Basson, M.A., Gritli-Linde, A., Cobourne, M.T., Green, J.B.: Periodic stripe formation by a Turing mechanism operating at growth zones in the mammalian palate. Nat. Genet. **44**, 348–351 (2012). doi:10.1038/ng.1090
25. Elmhirst, T.: $\mathbb{S}_N$-equivariant symmetry-breaking bifurcations. Int. J. Bifurc. Chaos **14**, 1017–1036 (2004)
26. Elmhirst, T., Doebeli, M., Stewart, I.: Pod systems: an equivariant ordinary differential equation approach to dynamical systems on a spatial domain. Nonlinearity **24**, 1507–1531 (2008)
27. Ermentrout, G.B., Cowan, J.D.: A mathematical theory of visual hallucination patterns. Biol. Cybern. **4**, 137–150 (1979)
28. Faye, G., Chossat, P.: Bifurcation diagrams and heteroclinic networks of octagonal H-planforms. J. Nonlinear Sci. **22**, 277–325 (2012). doi:10.1007/s00332-011-9118-x
29. Field, M., Golubitsky, M.: Symmetry in Chaos. Oxford University Press, Oxford (1992)
30. Field, M., Melbourne, I., Nicol, M.: Symmetric attractors for diffeomorphisms and flows. Proc. Lond. Math. Soc. **72**, 657–696 (1996)

31. FitzHugh, R.: Impulses and physiological states in theoretical models of nerve membrane. Biophys. J. **1**, 445–466 (1961)
32. Fulton, W.: Algebraic Curves. Benjamin, New York (1974)
33. Gambaryan, P.P.: How Mammals Run: Anatomical Adaptations. Wiley, New York (1974)
34. Golubitsky, M., Knobloch, E., Stewart, I.: Target patterns and spirals in planar reaction–diffusion systems. J. Nonlinear Sci. **10**, 333–354 (2000)
35. Golubitsky, M., Romano, D., Wang, Y.: Network periodic solutions: full oscillation and rigid synchrony. Nonlinearity **23**, 3227–3243 (2010)
36. Golubitsky, M., Romano, D., Wang, Y.: Network periodic solutions: patterns of phase-shift synchrony. Nonlinearity **25**, 1045–1074 (2012)
37. Golubitsky, M., Shiau, L.J., Stewart, I.: Spatio-temporal symmetries in the disynaptic canal-neck projection. SIAM J. Appl. Math. **67** (2007). doi:10.1137/060667773
38. Golubitsky, M., Shiau, L.J., Török, A.: Bifurcation on the visual cortex with weakly anisotropic lateral coupling. SIAM J. Appl. Dyn. Syst. **2**, 97–143 (2003)
39. Golubitsky, M., Stewart, I.: The Symmetry Perspective. Birkhäuser, Basel (2002)
40. Golubitsky, M., Stewart, I., Buono, P.-L., Collins, J.J.: A modular network for legged locomotion. Phys. D **115**, 56–72 (1998)
41. Golubitsky, M., Stewart, I., Buono, P.-L., Collins, J.J.: Symmetry in locomotor central pattern generators and animal gaits. Nature **401**, 693–695 (1999)
42. Golubitsky, M., Stewart, I., Schaeffer, D.G.: Singularities and Groups in Bifurcation Theory, vol. 2, Applied Mathematical Sciences 69. Springer, New York (1988)
43. Gray, J.: Animal Locomotion. Weidenfeld and Nicholson, London (1968)
44. Greenberg, M.J.: Euclidean and Non-Euclidean Geometries: Development and History. W.H. Freeman, New York (2008)
45. Grillner, S., Parker, D., El Manira, A.J.: Vertebrate locomotion—a lamprey perspective. Ann. N. Y. Acad. Sci. **860**, 1–18 (1998)
46. Grillner, S., Wallén, P.: Central pattern generators for locomotion, with special reference to vertebrates. Ann. Rev. Neurosci **8**, 233–261 (1985)
47. Guckenheimer, J., Holmes, P.: Nonlinear Oscillations, Dynamical Systems, and Bifurcations of Vector Fields. Springer, New York (1983)
48. Higashi, M., Takimoto, G., Yamamura, N.: Sympatric speciation by sexual selection. Nature **402**, 523–526 (1999)
49. Hofbauer, J., Sigmund, K.: Evolutionary Games of Population Dynamics. Cambridge University Press, Cambridge (1998)
50. Höfer, T.: Modelling dyctyostelium aggregation. D.Phil Thesis, Oxford University, Oxford (1996)
51. Hoppensteadt, F.: An Introduction to the Mathematics of Neurons. Cambridge University Press, Cambridge (1986)
52. Humphreys, J.E.: Reflection Groups and Coxeter Groups, Cambridge Studies in Advanced Mathematics 29. Cambridge University Press, Cambridge (1992)
53. Ikeda, K., Murota, K., Akamatsu, T., Kono, T., Takayama, Y., Sobhaninejad, G., Shibasaki, A.: Self-organizing hexagons in economic agglomeration: coreperiphery models and central place theory. Mathematical Engineering Technical Reports METR-2010-28, Department of Mathematics, University of Tokyo (2010)
54. Ikeda, K., Murota, K., Takashi, A., Kono, T., Takayama, Y.: Self-organizing hexagons for core-periphery models: central place theory and group theory. Mathematical Engineering Technical Reports METR-2011-24, Department of Mathematics, University of Tokyo (2011)
55. Ikeda, K., Murota, K., Takashi, A.: Self-organization of Lösch's hexagons in economic agglomeration for core-periphery models. Mathematical Engineering Technical Reports METR 2011-15, Dept. of Mathematical Informatics, University of Tokyo (2011)
56. Iooss, G., Joseph, D.D.: Elementary Stability and Bifurcation Theory, 2nd edn. Springer, New York (1990)
57. Kawecki, T.J.: Sympatric speciation via habitat specialization driven by deleterious mutations. Evolution **51**, 1751–1763 (1997)
58. Keef, T., Twarock, R.: Affine extensions of the icosahedral group with applications to the three-dimensional organisation of simple viruses. J. Math. Biol. **59**, 287–313 (2009)
59. Kirchgässner, K.: Exotische Lösungen des Bénardschen Problems. Math. Methods Appl. Sci. **1**, 453–467 (1979)

60. Kisdi, E., Geritz, S.A.H.: Adaptive dynamics in allele space: evolution of genetic polymorphism by small mutations in a heterogeneous environment. Evolution **53**, 993–1008 (1999)
61. Klüver, H.: Mescal and Mechanisms of Hallucinations. University of Chicago Press, Chicago (1966)
62. Kondo, S., Asai, R.: A reaction–diffusion wave on the skin of the marine angelfish *Pomacanthus*. Nature **376**, 765–768 (2002). doi:10.1038/376765a0
63. Kondrashov, A.S., Kondrashov, F.A.: Interactions among quantitative traits in the course of sympatric speciation. Nature **400**, 351–354 (1999)
64. Kopell, N., Ermentrout, G.B.: Symmetry and phaselocking in chains of weakly coupled oscillators. Comm. Pure Appl. Math. **39**, 623–660 (1986)
65. Kopell, N., Ermentrout, G.B.: Coupled oscillators and the design of central pattern generators. Math. Biosci. **90**, 87–109 (1988)
66. Krinsky, V.I.: Mathematical models of cardiac arrhythmias (spiral waves). Pharm. Ther. B **3**, 539–555 (1978)
67. Krinsky, V.I., Medvinskii, A.B., Parfilov, A.V.: Evolutionary autonomous spiral waves (in the heart). Math. Cybern. Pop. Ser. (Life Sci.) **8**, 1–48 (1986)
68. Krugman, P.: The Self-Organizing Economy. Blackwell, Malden (1996)
69. Lamb, J.S.W.: Reversing symmetries in dynamical systems. J. Phys. A **25**, 925–937 (1992)
70. Liddington, R.C., Yan, Y., Moulai, J., Sahli, R., Benjamin, T.L., Harrison, S.C.: Structure of simian virus 40 at 3.8-Å resolution. Nature **354**, 278–284 (1991)
71. Lösch, A.: The Economics of Location. Yale University Press, London (1954)
72. Macdonald, I.D.: The Theory of Groups. Clarendon Press, Oxford (1968)
73. Mayr, E.: Animal Species and Evolution. Harvard University Press, Cambridge (1963)
74. McCollum, G., Boyle, R.: Rotations in a vertebrate setting: evaluation of the symmetry group of the disynaptic canal-neck projection. Biol. Cybern. **90**, 203–217 (2004)
75. McNally, J.G., Cox, E.C.: Spots and stripes: the patterning spectrum in the cellular slime mould *Polysphondylium pallidium*. Development **105**, 323–333 (1989)
76. Meller, J.: The Buckminster Fuller Reader. Jonathan Cope, London (1970)
77. Mosekilde, E., Maistrenko, Y., Postonov, D.: Chaotic Synchronization. World Scientific, Singapore (2002)
78. Munz, M., Weidlich, W.: Settlement formation, part II: numerical simulation. Ann. Reg. Sci. **24**, 177–196 (1990)
79. Murray, J.D.: Mathematical Biology. Springer, Berlin (1989)
80. Nagata, W., Harrison, L.G., Wehner, S.: Reaction–diffusion models of growing plant tips: bifurcations on hemispheres. Bull. Math. Biol. **65**, 571–607 (2003)
81. Nagumo, J.S., Arimoto, S., Yoshizawa, S.: An active pulse transmission line simulating nerve axon. Proc. IRE **50**, 2061–2071 (1962)
82. Ridley, M.: Evolution. Blackwell, Oxford (1996)
83. Rundle, H.D., Nagel, L., Boughman, J.W., Schluter, D.: Natural selection and parallel speciation in sympatric sticklebacks. Science **287**, 306–308 (2000)
84. Sattinger, D.H.: Group representation theory, bifurcation theory and pattern formation. J. Funct. Anal. **28**, 58–101 (1978)
85. Sattinger, D.H., Weaver, O.L.: Lie Groups and Algebras with Applications to Physics, Geometry and Mechanics. Springer, New York (1986)
86. Schwartz, E.: Spatial mapping in the primate sensory projection: analytic structure and relevance to projection. Biol. Cybern. **25**, 181–194 (1977)
87. Seger, J.: Intraspecific resource competition as a cause of sympatric speciation. In: Greenwood, P.J., Harvey, P.H., Slatkin, M. (eds.) Evolution. Cambridge University Press, Cambridge (1985)
88. Sheth, R., Marcon, L., Bastida, F., Junco, M., Quintana, L., Dahn, R., Kmita, M., Sharpe, J., Ros, M.: Hox genes regulate digit patterning by controlling the wavelength of a Turing-type mechanism. Science **338**, 1476–1480 (2012). doi:10.1126/science.1226804
89. Sick, S., Reinker, S., Timmer, J., Schlake, T.: WNT and DKK determine hair follicle spacing through a reaction–diffusion mechanism. Science **314**, 1447–1450 (2006). doi:10.1126/science.1130088
90. Stewart, I.: Self-organization in evolution: a mathematical perspective. Philos. Trans. R. Soc. Lond. A **361**, 1101–1123 (2003)
91. Stewart, I., Elmhirst, T., Cohen, J.: Symmetry-breaking as an origin of species. In: Buescu, J., Castro, S.B.S.D., Dias, A.P.S., Labouriau, I.S. (eds.) Bifurcations, Symmetry and Patterns, pp. 3–54. Birkhäuser, Basel (2003)

92. Stewart, I., Parker, M.: Periodic dynamics of coupled cell networks I: rigid patterns of synchrony and phase relations. Dyn. Syst. **22**, 389–450 (2007)
93. Stewart, I., Parker, M.: Periodic dynamics of coupled cell networks II: cyclic symmetry. Dyn. Syst. **23**, 17–41 (2008)
94. Tachikawa, M.: Specific locking in populations dynamics: symmetry analysis for coupled heteroclinic cycles. J. Comput. Appl. Math. **201**, 374–380 (2007)
95. Tregenza, T., Butlin, R.K.: Speciation without isolation. Nature **400**, 311–312 (1999)
96. Turing, A.M.: The chemical basis of morphogenesis. Philos. Trans. Roy. Soc. Lond. B **237**, 32–72 (1952)
97. Twarock, R.: A tiling approach to virus capsid assembly explaining a structural puzzle in virology. J. Theor. Biol. **226**, 477–482 (2004)
98. Twarock, R.: A mathematical physicist's approach to the structure and assembly of viruses. Philos. Trans. R. Soc. Lond. A **364**, 3357–3374 (2006)
99. Vanderbauwhede, A.: Local Bifurcation and Symmetry. Pitman, Boston (1982)
100. Vincent, T.L., Vincent, T.L.S.: Evolution and control system design. IEEE Control Syst. Mag, pp. 20–35 (2000)
101. Wikipedia. http://en.wikipedia.org/wiki/Spontaneous_symmetry_breaking
102. Wilson, H.R., Cowan, J.D.: Excitatory and inhibitory interactions in localized populations of model neurons. Biophys. J. **12**, 1–24 (1972)
103. Wilson, H.R., Cowan, J.D.: A mathematical theory of the functional dynamics of cortical and thalamic nervous tissue. Kybernetik **13**, 55–80 (1973)
104. Winfree, A.T.: Sudden cardiac death: a problem in topology. Sci. Am. **248**, 144–161 (1983)
105. Wolpert, L.: Positional information and the spatial pattern of cellular differentiation. J. Theor. Biol. **25**, 1–47 (1969). doi:10.1016/S0022-5193(69)80016-0
106. Wrigley, N.G.: An electron microscope study of the structure of Sericesthis iridescent virus. J. Gen. Virol. **5**, 123–134 (1969)
107. Wrigley, N.G.: An electron microscope study of the structure of Tipula iridescent virus. J. Gen. Virol. **5**, 169–173 (1970)